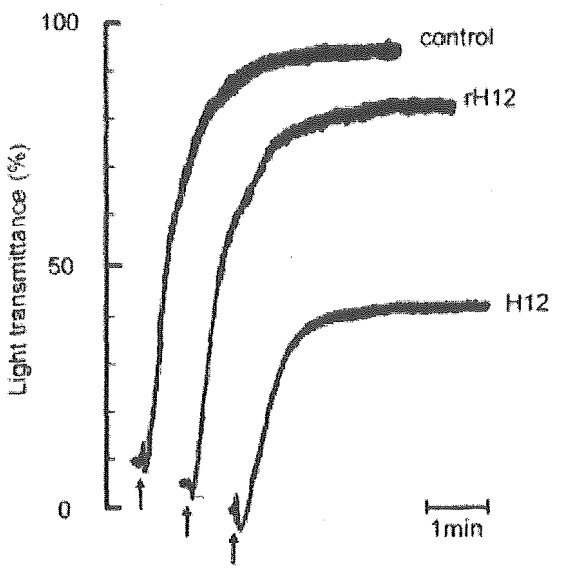

Fig. 1. ADP-induced (20 μmol/L) PLT aggregation (200×10^3/μL) was monitored with an aggregometer in the presence of 1 mmol per L H12, cH12, or PBS (control).

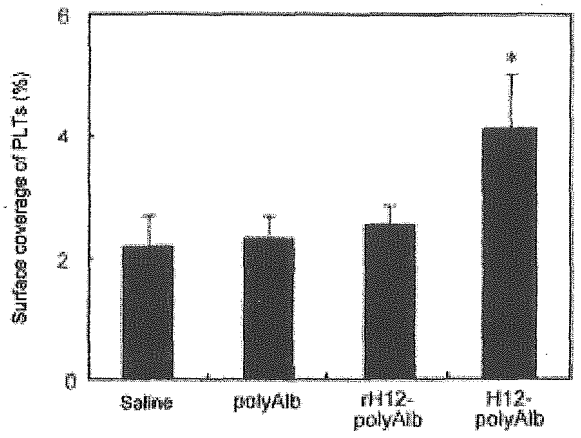

Fig. 2. Comparison of surface coverage of PLTs in the thrombocytopenic imitation blood on the collagen surface after addition of H12-polyAlb, cH12-polyAlb, or polyAlb at a shear rate of 150 per second (n = 4). The amount of surface coverage was recorded after blood was circulated for 210 seconds. The concentration of PLTs was 20×10^3 per μL. *$p < 0.05$ for the H12-polyAlb group versus the saline group, the polyAlb group, and the cH12-polyAlb group.

tion.[31] In particular, when H12 was added at a concentration of 1 mmol per L, PLT aggregation was significantly suppressed in comparison with the control experiment (Fig. 1). In contrast, cH12 at the same concentration did not inhibit PLT aggregation.

Characterization of H12-polyAlb and cH12-polyAlb

In the conjugation reaction, the mercapto group of the terminal cysteine of H12 or cH12 reacted with the pyridyl disulfide–bonded group of the polyAlb, which have diameters of 260 ± 60 nm, and 2-thiopyridone was liberated after the formation of disulfide linkage owing to the thiol-disulfide exchange reaction. With the absorption of the liberated 2-thiopyridone at 343 nm, the number of the H12 and cH12 molecules conjugated to one polyAlb was estimated to be approximately 9.6×10^3 and 9.1×10^3, respectively. The endotoxin concentration in the H12- or cH12-polyAlb suspension was below 0.2 EU per mL.

Measurement of the interaction of PLTs with the collagen surface in the presence of H12-polyAlb with thrombocytopenic imitation blood under flow conditions

We prepared the thrombocytopenic imitation blood and adjusted the number of PLTs to 20×10^3 per μL. The PLTs were labeled with a fluorescent marker, 3,3′-dihexyloxacarbocyanine iodide, to observe the adherence of PLTs to the collagen surface at a shear rate of 150 per second. In the presence of the control polyAlb, the total surface coverage of PLTs was 2.1 ± 0.4 percent after 210 seconds of flow (Fig. 2). When PLTs were allowed to flow over the collagen-immobilized surface in the absence of polyAlb, the same value was obtained. When the H12-polyAlb were added to the blood instead of the polyAlb, there was a significant increase in the surface coverage to 3.9 ± 1.1 percent. By contrast, when cH12-polyAlb was used, the surface coverage did not change from that of the control polyAlb (2.4 ± 0.4%).

Preparation of the thrombocytopenic rats

Rats that received busulfan at total doses of 40 or 30 mg per kg developed profound thrombocytopenia with a decline in the level of PLTs to half-maximal value on Day 7 or 8, respectively, which reached the lowest value between Day 10 and Day 14 (Fig. 3). Unfortunately, the rats became anorexic, lost weight, became anemic, and were all dead by Days 12 and 16, respectively (data not shown). At a total dose of 20 mg per kg, however, thrombocytopenia was just as profound as at the higher doses of busulfan, but all rats survived with no major problems. As shown in Fig. 3, the rats treated with the 20 mg per kg dose had a decline in PLT count to half-maximal value ($410 \times 10^3 \pm 30 \times 10^3$/μL) on Day 9. On Day 10, their PLT concentration was $200 \times 10^3 \pm 30 \times 10^3$ per μL, which was equivalent to one-fourth to one-fifth of the PLT count of normal rats. There was a slight decrease in the WBCs concentration of the busulfan-treated rats compared with that of uninjected

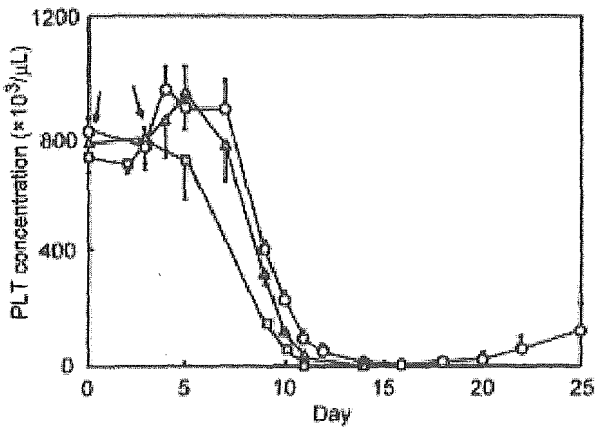

Fig. 3. Dose-response effect of busulfan on rats. Rats were injected with busulfan at a total dose of 20 (○), 30 (△), or 40 mg per kg (□) as described under Materials and Methods. Tail vein blood was collected at intervals and PLT concentration measured. Arrows show injection day of busulfan (n = 5).

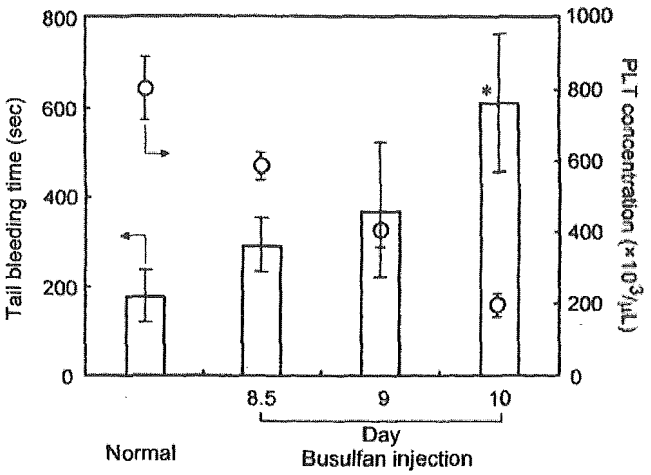

Fig. 4. Correlation of tail bleeding time (white bars) with PLT concentration (○) in the rat (n = 5). *p < 0.05 for the Day 10 group vs. the normal group.

TABLE 1. Weights and hematologic measures before and after (on Day 10) busulfan injection

Rat	Initial weight (g)	Final weight (g)	RBCs (×10³/μL)	WBCs (×10³/μL)	PLTs (×10³/μL)
Normal (n = 6)	251 ± 11	304 ± 15	7160 ± 300	12.7 ± 2.8	809 ± 86
Busulfan 20 mg/kg (n = 6)	258 ± 10	288 ± 12	7000 ± 230	8.1 ± 1.2	198 ± 28

control rats; however, the weight of busulfan-injected rats increased and their RBC counts were unchanged (Table 1). Predictably, there was a gradual decrease in the PLT count of the busulfan-treated rats to Day 11 ($97 \times 10^3 \pm 25 \times 10^3$/μL); however, RBC count also began to decline compared with that of uninjected control rats (data not shown). After the PLT count reached the lowest point on Day 14, the low count of $3 \times 10^3 \pm 2 \times 10^3$ per μL persisted for at least 6 days before starting to increase gradually.

Measurement of the tail bleeding time of the thrombocytopenic rats in the presence of H12-polyAlb

The tail bleeding times of the normal rats ([PLT] = $810 \times 10^3 \pm 90 \times 10^3$/μL) and thrombocytopenic rats on Day 10 after the busulfan injection ([PLT] = $200 \times 10^3 \pm 30 \times 10^3$/μL) were 187 ± 51 and 609 ± 153 seconds, respectively (Fig. 4). In contrast, PLT concentrations in the course of preparation of thrombocytopenic rats on Days 8.5 and 9 were $570 \times 10^3 \pm 40 \times 10^3$ and $410 \times 10^3 \pm 30 \times 10^3$ per μL, respectively, and their bleeding time was 288 ± 56 and 366 ± 153 seconds, respectively. In addition, after Day 11, thrombocytopenia became progressive rapidly but the measurement of bleeding time was hard to be standardized (data not shown). In fact, the bleeding time of the busulfan (20 mg/kg)-injected rats on Day 11 (PLTs; $97 \times 10^3 \pm 25 \times 10^3$/μL) was found to be immeasurable, because bleeding did not stop for more than 30 minutes. Therefore, for in vivo experiment we used animals on Day 10 after the busulfan treatment.

The intravenous administration of H12-polyAlb at a dose of 1 mg per kg slightly reduced the bleeding time to 581 ± 110 seconds in comparison with those of saline group (609 ± 153 sec) or control polyAlb at a dose of 1 mg per kg (679 ± 102 sec) (Fig. 5). At doses of 4 and 10 mg per kg, we confirmed a dose-dependent reduction of the bleeding time, and the time decreased significantly to 342 ± 73 and 288 ± 120 seconds, respectively. By comparison, control polyAlb groups at doses of 4 and 10 mg per kg were 553 ± 104 and 436 ± 102 seconds, respectively.

DISCUSSION

In the previous studies on PLT substitutes[2-5] despite their usefulness in reinforcing PLT aggregation and reducing bleeding time in vivo, their raw materials are dependent on human blood. In our previous studies, we have focused on H12, which is a synthetic peptide of human fibrinogen, and we conjugated H12 to the surface of fluorescein isothiocyanate (FITC)-labeled latex beads.[31] H12-latex

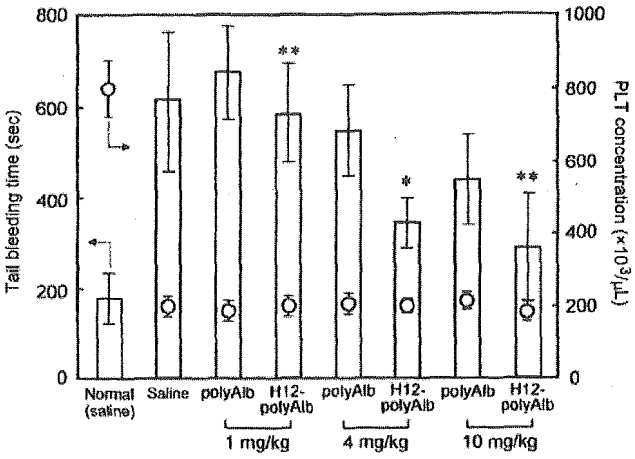

Fig. 5. Effects of the administration of H12-polyAlb on tail bleeding time (white bars). The administered amount of H12-polyAlb was 1, 4, and 10 mg/kg equivalent of albumin. (○) PLT concentration in the rats (n = 6-10). *p < 0.05 or **not significant for the H12-polyAlb group vs. the polyAlb group at the same dose.

beads in an RBC suspension were allowed to flow over the activated PLTs that were immobilized on a collagen surface at a shear rate of 150 per second. They adhered and accumulated to the surface in a time-dependent manner, whereas control latex beads did not adhere. The adhesion of H12-latex beads was suppressed in the presence of free H12 as an inhibitor of GPIIb/IIIa binding, showing that the adhesion was specific. Furthermore, the H12-latex beads showed minimal interaction with nonactivated PLTs based on the results of flow cytometric analyses of agglutination with the FITC-labeled latex beads. Therefore, H12 is a noninfective promising part as a recognition site of PLT substitutes. We prepared H12 particles with rHSA, which was not derived from human blood, to obtain information about the possibility to construct biocompatible and biodegradable particles with hemostatic ability in thrombocytopenic conditions.

First, we confirmed a specific binding of H12 in comparison with cH12 from a study of the inhibition of fibrinogen-mediated PLT aggregation. Because H12 is a fibrinogen sequence, which is responsible for the recognition of GPIIb/IIIa on activated PLTs,[22-28] it significantly suppressed the PLT aggregation by competitive binding to the fibrinogen-binding site of the PLT, and the binding of H12 for GPIIb/IIIa was maintained even after the introduction of the N-terminal cysteine. In contrast, cH12 showed a minimal inhibitory effect. These results were also supported by the other publications that the IC_{50} of inhibition of ^{125}I-fibrinogen binding to activated PLTs by H12 and cH12 was 28 and 85 μmol per L, respectively, indicating that binding avidity for GPIIb/IIIa of H12 was stronger than that of cH12.[23,24]

We sufficiently conjugated either H12 or cH12 to the surface of polyAlb and estimated the conjugation density on the polyAlb surface to approximately 46×10^3 or 43×10^3 molecules per μm^2, respectively. The conjugation densities were similar to that of H12-latex beads (diameter, 1 μm), which enhanced PLT thrombus formation.[31] In thrombocytopenic imitation blood flowing on the collagen surface, the surface coverage of PLTs in the presence of control polyAlb was very low and the same in the absence of polyAlb. Furthermore, we confirmed that H12-polyAlb enhanced the thrombus formation of the remaining PLTs, whereas cH12-polyAlb did not. They indicate that the particles such as the polyAlb and the cH12-polyAlb did not interfere the PLT adhesion and aggregation, and the enhancement effect was specific for H12 conjugated to the surface of polyAlb.

Next, we prepared the thrombocytopenic rats with busulfan to evaluate a hemostatic ability of H12-polyAlb in vivo. We succeeded in obtaining the extinction curve of PLTs similar to that of the previous studies.[32] It was reported that a low hematocrit resulted in a significant prolongation in the bleeding time.[34] In fact, the bleeding time of the busulfan (20 mg/kg)-injected rats on Day 11 (PLTs; $97 \times 10^3 \pm 25 \times 10^3$/μL) was found to be immeasurable, because bleeding did not stop for more than 30 minutes. From the data of hematologic indices, in which the PLT counts were sufficiently decreased and the RBC counts were maintained, as shown in Table 1, we determined that the appropriate dose of busulfan for the rats was 20 mg per kg and the incision of the tail was to be made on Day 10. The bleeding time of the thrombocytopenic rats on Day 10 was extended significantly in comparison with that of normal rats as shown in Fig. 4. The bleeding time approached that of normal rats as their PLT concentration increased. We confirmed that the bleeding time was correlated with their PLT concentration and inferred that the tail bleeding time was an effective evaluation measure for measuring the hemostatic capacity of the PLT substitutes.

The endotoxin concentration in the H12- or cH12-polyAlb suspension was below 0.2 EU per mL, acceptable for the in vivo study. In preliminary experiments we studied the systemic clearance of H12-polyAlb. At a dose of 4 mg per kg (equivalent albumin concentration), the amount of FITC-labeled H12-polyAlb rapidly decreased to 88.8, 51.1, 27.2, and 9.0 percent after 5, 10, 15, and 30 minutes, respectively (taken as 100% just after injection) with a spectrofluorometer (FP-750, Jasco, Tokyo, Japan). The half-life of the H12-polyAlb was estimated to be approximately 10 minutes from the above data. Therefore, we measured the tail bleeding time 5 minutes after the injection. We are now studying the prolongation of the half-life of the H12-polyAlb with PEG modification.

Although not tested in animals with severe thrombocytopenia, we confirmed the hemostatic effect of H12-

polyAlb in vivo with moderately thrombocytopenic rats, suggesting that the polyAlb may be a promising candidate for PLT substitutes (Fig. 5). The circulating H12-polyAlb at the dose of 4 mg per kg significantly reduced the bleeding time of the thrombocytopenic rats, whereas at a lower concentration of 1 mg per kg, the hemostatic effect did not reach a significant level. At a higher concentration of 10 mg per kg, however, the bleeding time of H12-polyAlb was significantly reduced in comparison with that of saline group, but not the polyAlb group, because the bleeding time of the control polyAlb was also slightly reduced, indicating that the polyAlb itself possessed a hemostatic activity at its higher concentration. When we used PEG-modified polyAlb, the bleeding time became comparable to that obtained with saline group (manuscript in preparation), suggesting that negative charge of the control polyAlb at pH 7.4 may nonspecifically cause the shortening of the tail bleeding time.

We estimated that the hemostatic ability of the H12-polyAlb at a dose of 4 mg per kg (approx. 1.0×10^{11} particles) would correspond to 1/20th of the hemostatic ability of one PLT, which was based on the bleeding time of the thrombocytopenic rats and PLT concentration. Furthermore, we confirmed that hematologic indices were stable before and after the administration of H12-polyAlb.

In conclusion, H12-polyAlb was shown to preferentially interact with an activated PLT surface via GPIIb/IIIa receptors and to facilitate PLT accumulation at sites of hemostasis. Furthermore, H12-polyAlb had the hemostatic ability in the tail bleeding model of thrombocytopenic rats. Thus, H12-polyAlb may be a suitable candidate for an alternative to human PLT concentrates infused into thrombocytopenic patients.

ACKNOWLEDGMENTS

The authors thank M. Murata, M.D., Ph.D. and K. Yokoyama, M.D., Ph.D. at Keio University for useful discussion about the functional evaluation of H12 peptide.

REFERENCES

1. Graham SS, Gonchoroff NJ, Miller JL. Infusible platelet membranes retain partial functionality of the platelet GPIb/IX/V receptor complex. Am J Clin Pathol 2001;115:144-7.
2. Rybak M, Renzulli LA. A liposome based platelet substitutes, the plateletsome, with hemostatic efficacy. Biomater Artif Cells Immobil Biotechnol 1993;21:108-18.
3. Agam G, Livine AA. Erythrocytes with covalently bound fibrinogen as a cellular replacement for the treatment of thrombocytopenia. Eur J Clin Invest 1992;22:105-12.
4. Levi M, Friedrich PW, Middleton S, et al. Fibrinogen-coated albumin microcapsules reduce bleeding in severely thrombocytopenic rabbits. Nat Med 1999;5:107-11.
5. Coller BS, Springer KT, Beer JH, et al. Thromboerythrocytes: in vitro studies of a potential autologous, semi-artificial alternative to platelet transfusion. J Clin Invest 1992;89:546-55.
6. Ikeda Y, Handa M, Kawano K, et al. The role of von Willebrand factor and fibrinogen in platelet aggregation under varying shear stress. J Clin Invest 1991;87:1234-40.
7. Santro SA, Zutter MM. The α2β1integrin: a collagen receptor on platelets and other cells. Thromb Hemost 1995;74:813-21.
8. Sixma JJ, van Zanten GH, Huizinga EG, et al. Platelet adhesion to collagen: an update. Thromb Hemost 1997;78:434-8.
9. Marchese P, Saldivar E, Ware J, Ruggeri ZM. Adhesive properties of the isolated amino-terminal domain of platelet glycoprotein Ibα in a flow field. Proc Natl Acad Sci U S A 1999;96:7837-42.
10. Kitaguchi T, Murata M, Iijima K, et al. Characterization of liposomes carrying von Willebrand factor-binding domain of platelet glycoprotein Ibα: a potential substitute for platelet transfusion. Biochem Biophys Res Commun 1999;261:784-9.
11. Teramura Y, Okamura Y, Takeoka S, et al. Hemostatic effects of polymerized albumin particles bearing rGPIa/IIa in thrombocytopenic mice. Biochem Biophys Res Commun 2003;306:256-60.
12. Nishiya T, Murata M, Handa M, Ikeda Y. Targetting of liposomes carrying recombinant fragments of platelet membrane glycoprotein Ibα to immobilized von Willebrand factor under flow conditions. Biochem Biophys Res Commun 2000;270:755-60.
13. Nishiya T, Kainoh M, Murata M, Handa M, Ikeda Y. Reconstitution of adhesive properties of human platelets in liposomes carrying both recombinant glycoproteins Ia/IIa and Ibα under flow conditions: specific synergy of receptor–ligand interactions. Blood 2002;100:136-42.
14. Takeoka S, Teramura Y, Okamura Y, et al. Fibrinogen-conjugated albumin polymers and their interaction with platelets under flow conditions. Biomacromolecules 2001;2:1192-7.
15. Takeoka S, Teramura Y, Ohkawa H, Ikeda Y, Tsuchida E. Conjugation of von Willebrand factor-binding domain of platelet glycoprotein Ibα to size-controlled albumin microsheres. Biomacromolecules 2000;1:290-5.
16. Takeoka S, Teramura Y, Okamura Y, et al. Rolling properties of rGPIbα-conjugated phospholipid vesicles with different membrane flexibilities on vWf surface under flow conditions. Biochem Biophys Res Commun 2002;296:765-70.
17. Takagi J, Petre BM, Walz T, Springer TA. Global comformational rearrangemrents in integrin extracellular domains in outside-in and inside-out signaling. Cell 2002;110:599-611.
18. Marguerie GA, Plow EF, Edgington TS. Human platelets possess an inducible and saturable receptor specific for fibrinogen. J Biol Chem 1979;254:5357-63.

19. Ruggeri ZM, De Marco L, Gatti L. Platelets have more than one binding site for von Willebrand factor. J Clin Invest 1983;72:1-12.
20. Mustard JF, Packham MA, Kinlough-Rathbone RL. Fibrinogen and ADP-induced platelet aggregation. Blood 1978;52:453-66.
21. De Marco L, Girolami A, Zimmerman TS. Von Willebrand factor interaction with the glycoprotein IIb/IIIa complex. J Clin Invest 1986;77:1272-7.
22. Hawiger J, Kloczewiak M, Bednarek MA, Timmons S. Platelet receptor recognition domains on the α chain of human fibrinogen: structure-function analysis. Biochemistry 1989;28:2909-14.
23. Kloczewiak M, Timmons S, Hawiger J. Localization of a site interacting with human platelet receptor on carboxy-terminal segment of human fibrinogen γ chain. Biochem Biophys Res Commun 1982;107:181-7.
24. Kloczewiak M, Timmons S, Lukas TJ, Hawiger J. Platelet receptor recognition site on human fibrinogen: synthesis and structure-function relationship of peptides corresponding to the carboxy-terminal segment of the γ chain. Biochemistry 1984;23:1767-74.
25. Kloczewiak M, Timmons S, Bednarek MA, Sakon M, Hawiger J. Platelet receptor recognition domain on the g chain of human fibrinogen and its synthetic peptide analogues. Biochemistry 1989;28:2915-9.
26. Phillips DR, Charo IF, Scarborough RM. GPIIb-IIIa: the responsive integrin. Cell 1991;65:359-62.
27. Lam SC, Plow EF, Smith MA, et al. Evidence that arginyl-glycyl-aspartate peptides and γ chain peptides share a common binding site on platelets. J Biol Chem 1987; 262:110-5.
28. Hallahan DE, Geng L, Cmelak AJ, et al. Targeting drug delivery to radiation-induced neoantigens in tumor microvasculature. J Control Release 2001;74:183-91.
29. Bonnefoy A, Liu Q, Legrand C, Frojmovic MM. Efficiency of platelet adhesion to fibrinogen depends on both cell activation and flow. Biophys J 2000;78:2834-43.
30. Beer JH, Springer KT, Coller BS. Immobilized Arg-Gly-Asp (RGD) peptides of varying lengths as structural probes of the platelet glycoprotein IIb/IIIa receptor. Blood 1992;79:117-28.
31. Takeoka S, Okamura Y, Teramura Y, et al. Function of fibrinogen γ-chain dodecapeptide-conjugated latex beads under flow. Biochem Biophys Res Commun 2003;312:773-9.
32. Yang C, Li YC, Kuter DJ. The physiological response of thrombopoietin (c-Mpl ligand) to thrombocytopenia in the rat. Br J Hematol 1999;105:478-85.
33. Stenberg PE, Barrie RJ, Pestina TI, et al. Prolonged bleeding time with defective platelet filopodia formation in the Wistar Furth rat. Blood 1998;91:1599-608.
34. Sola MC, del Vecchio A, Edwards TJ, et al. The relationship between hematocrit and bleeding time in very low birth weight infants during the first week of life. J Perinatol 2001;21:368-71.

Hemostatic Effects of Phospholipid Vesicles Carrying Fibrinogen γ Chain Dodecapeptide in Vitro and in Vivo

Yosuke Okamura,[†,§] Ippei Maekawa,[†] Yuji Teramura,[†] Hitomi Maruyama,[‡] Makoto Handa,[§] Yasuo Ikeda,[‡] and Shinji Takeoka*[,†]

Graduate School of Science and Engineering, Waseda University, Tokyo, 169-8555, Japan, Department of Internal Medicine, School of Medicine, Keio University, Tokyo, 160-8582, Japan, and Department of Transfusion Medicine & Cell Therapy, School of Medicine, Keio University, Tokyo, 160-8582, Japan. Received June 21, 2005; Revised Manuscript Received September 15, 2005

We studied prototypes of platelet substitutes that bear on their surface a dodecapeptide, HHLGGAKQAGDV (H12). The peptide is a fibrinogen γ chain carboxy-terminal sequence (γ400–411) and recognizes specifically the active form of glycoprotein (GP) IIb/IIIa on the surface of activated platelets. We conjugated H12 to the end of poly(ethylene glycol) chains on the surface of a phospholipid vesicle with an average diameter of 220 nm to prepare H12–PEG–vesicles. The half-life of the H12–PEG–vesicles was significantly prolonged by PEG modification, and the ability of H12 on the surface of the vesicle to recognize GPIIb/IIIa was maintained even though the surface was modified with PEG chains. The H12–PEG–veiscles enhanced the in vitro thrombus formation of platelets that were adhering to a collagen-immobilized plate, when thrombocytopenia-imitation blood was passed over the plate. Based on the flow cytometric analyses of PAC-1 binding and P-selectin expression, the H12–PEG–vesicles were shown not to cause platelet activation. Furthermore, the H12–PEG–vesicles dose-dependently shortened the tail bleeding time of thrombocytopenic rats. It was confirmed that the H12–PEG–vesicles had a hemostatic effect and may be a suitable candidate for an alternative to human platelet concentrates transfused into thrombocytopenic patients.

INTRODUCTION

Platelet transfusion plays an important role in prophylactic therapy for patients with thrombocytopenia caused by hematologic malignancies or intensive chemotherapy for solid tumors or as a result of surgical procedures and radiotherapy. However, due to the short storage life of platelets (3 days in Japan), the shortage has become a serious concern in an aging society. Furthermore, the risk of viral and bacterial infections accompanied by transfusion is also a serious issue. To solve these problems, various platelet substitutes (*1*) have been developed, such as, solubilized platelet membrane protein-conjugated liposomes (Plateletsome) (*2*), infusible platelet membranes (IPM) (*3*), fibrinogen-coated albumin microcapsules (Synthocyte) (*4*), fibrinogen-bonded red blood cells (*5*), liposomes bearing fibrinogen (*6*), and arginine-glycine-aspartic acid (RGD) peptide-bound red blood cells (Thromboerythrocyte) (*7*). These platelet substitutes consist of materials derived from blood components.

We have developed platelet substitutes using polymerized albumin particles (polyAlb) (*8–11*) and phospholipid vesicles (*12–15*) as biocompatible and biodegradable carriers and shown that those carriers carrying recombinant fragments of platelet membrane proteins (rGPIbα (*16*, *17*) and rGPIa/IIa complex (*18*, *19*)) specifically interact with a surface that mimics the site of bleeding injury, such as von Willebrand factor (VWF) and collagen immobilized on a surface under flow conditions in vitro. Moreover, we demonstrated that rGPIa/IIa-conjugated polyAlb reduced the tail bleeding time of thrombocytopenic mice (*8*). These carriers have the ability to induce platelet hemostasis; however, they cannot recruit flowing platelets to induce platelet aggregation.

When platelets are made to adhere to collagen immobilized on a surface and activated, the conformation of GPIIb/IIIa which exists on the platelet membrane changes from a silent form to an activated form (*20–22*). The activated form acts as a receptor for fibrinogen and VWF (*23–25*), which is followed by platelet aggregation (*26*, *27*). This is because fibrinogen contains three putative platelet interaction sites, namely, a tetrapeptide containing RGD sequences such as RGDF and RGDS at α95–98 and α572–575, respectively, and a dodecapeptide (HHLGGAKQAGDV, H12) at a γ chain carboxy-terminal segment (γ400–411) (*28*).

To study the usefulness of fibrinogen as a recognition site of platelet substitutes, we prepared fibrinogen-conjugated polyAlb, and we confirmed that the polyAlb enhanced adhesion of the flowing platelets to an activated platelet-immobilized surface in vitro (*9*). However, fibrinogen is derived from human blood and when isolated in solution tends to precipitate at 4 °C within a few hours (*29*).

Recently, we have focused on the stable dodecapeptide, H12, instead of fibrinogen (*28*, *30–33*). Based on our results obtained from flow cytometric analyses of agglutination, H12-conjugated latex beads showed minimal interaction with nonactivated platelets in comparison

* To whom correspondence should be addressed. E-mail: takeoka@waseda.jp. Tel: +813-5286-3217. Fax: +813-5286-3217.
† Graduate School of Science and Engineering, Waseda University.
§ Department of Transfusion Medicine & Cell Therapy, School of Medicine, Keio University.
‡ Department of Internal Medicine, School of Medicine, Keio University.

10.1021/bc050178g CCC: $30.25
Published on Web 11/01/2005

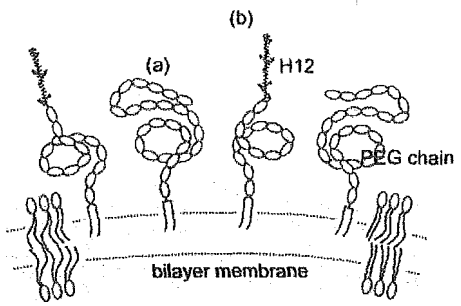

Figure 1. The structure of H12–PEG–vesicles: (a) PEG–DSPE (PEG 5.0 kDa) and (b) H12–PEG–Glu2C18 (PEG: 3.1 kDa, H12: 1.3 kDa) are incorporated into the bilayer membrane.

with RGD-conjugated latex beads (*34*). Furthermore, the H12-conjugated latex beads enhanced in vitro thrombus formation on the collagen-immobilized plate when thrombocytopenia-imitation blood was passed over the plate (*34*).

Phospholipid vesicles have been extensively studied as carriers for biologically important substances such as drugs, hemoglobin, enzymes, hormones, and DNA. In particular, recognition proteins such as antibodies and various ligands have been conjugated to the surface of vesicles to bind and interact with tissue epitopes or specific cells. Recently, it was reported that H12-liposomes enhanced platelet aggregation and specifically adhered to the platelets activated on the collagen surface in a state of rest (*35*). On the other hand, poly(ethylene glycol) (PEG) modification of the surface of the vesicles has been widely used to prolong the half-life or to stabilize their dispersion states (*36–40*). We previously reported that PEG modification of the vesicles was effective in preventing intervesicular access and aggregation as determined using a capillary viscosimeter and optical microscopy. Also, subcutaneous microvascular studies showed that PEG conjugates significantly improved microcirculation (flow rate, functional capillary density, and vessel diameter) (*38*, *39*).

In this study, we prepared phospholipid vesicles carrying both H12 and PEG chains to enhance the biocompatibility as a platelet substitute and to enhance the stabilization of the vesicles in vitro and in vivo, as noted above. Our purpose was to produce a platelet substitute for the indication of prophylactic transfusion. However, the excluded volume effect of the neighboring PEG chains might shield the recognition ability of H12. Therefore, we conjugated H12 to the end of the PEG chain by using PEG–lipids and prepared the PEG-modified vesicles carrying H12 (H12–PEG–vesicles, Figure 1). Then we studied the recognition ability toward platelets activated on collagen immobilized on a surface when thrombocytopenia-imitation blood was passed over the surface. Furthermore, we intravenously administered the H12–PEG–vesicles into thrombocytopenic rats and measured the tail bleeding time for evaluation of the hemostatic ability of the vesicles.

MATERIALS AND METHODS

Materials. All reagents were used without further purification. L-Glutamic acid, *p*-toluenesulfonic acid monohydrate (*p*-Tos), stearyl alcohol, and *N,N'*-dicyclohexylcarbodiimide were purchased from Kanto Chemical (Tokyo). 1,2-Distearoyl-*sn*-glycero-3-phosphatidylethanolamine-*N*-[monomethoxy poly(ethylene glycol)] (5000) (PEG–DSPE, M_w = 5.1 kDa), and α-maleimidyl-ω-hydroxy succinimidyl poly(ethylene glycol) (MAL–PEG–NHS, M_w = 3.5 kDa) were purchased from NOF (Tokyo). 1,2-Dipalmitoyl-*sn*-glycero-3-phosphatidylcholine (DPPC) and cholesterol were purchased from Nippon Fine Chemical (Osaka). 1,5-Dihexadecyl-*N*-succinyl-L-glutamate (DHSG) was synthesized in our laboratory (*41*, *42*). A fibrinogen γ chain dodecapeptide (C-HHLGGAKQAGDV, Cys-H12) was synthesized with a solid-phase synthesizer by BEX (Tokyo). 3,3'-Dihexyloxacarbocyanine iodide ($DiOC_6$), which is a platelet fluorescent dye, and dioctadecyloxacarbocyanine perchlorate ($DiOC_{18}$), which is a vesicle fluorescent dye, were purchased from Molecular Probes (Eugene, OR). Collagen I-A (Cellmatrix) was purchased from Nitta Gelatine (Osaka). D-Phe-Pro-Arg-chloromethyl ketone (PPACK) was purchased from Calbiochem (San Diego, CA). FITC-labeled PAC-1, which is anti-GPIIb/IIIa antibody, and FITC-labeled anti-P-selectin (CD62P) antibody were obtained from Becton Dickinson (San Jose, CA) and BD-Pharmingen (San Diego, CA), respectively. Both busulfan and poly(ethylene glycol) (average molecular weight 400) were purchased from Sigma-Aldrich (St Louis, MO).

Scheme 1. Syntheses of H12–PEG-Glu2C18 (PEG 3.1 kDa, H12 1.3 kDa)

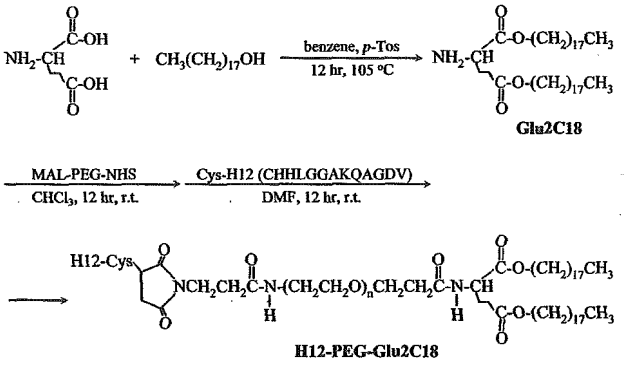

Synthesis of H12–PEG–Glu2C18. The syntheses were performed according to Scheme 1. L-Glutamic acid (2.96 g, 20 mmol) and *p*-Tos (4.56 g, 24 mmol) were dissolved in benzene and refluxed for 1 h at 105 °C. Stearyl alcohol was added to the solution, and the solution was refluxed for 12 h at 105 °C. The crude product was washed with an aqueous solution of saturated Na_2CO_3 and then distilled water. After recrystallization from methanol at 4 °C, 1,5-distearoyl-L-glutamate (Glu2C18) was obtained (9.5 g, yield 80%). Glu2C18 (115 mg, 176 μmol) and MAL–PEG–NHS (300 mg, 88 μmol) were dissolved in chloroform and stirred for 12 h at room temperature (rt). The crude product was purified by reprecipitation from diethyl ether. After recrystallization from ethanol, the MAL–PEG–Glu2C18 was obtained as a white solid (265 mg, yield 64%). MAL–PEG–Glu2C18 (100 mg, 25 μmol) and Cys-H12 (33 mg, 25 μmol) were reacted in *N,N*-dimethylformamide (DMF) for 12 h at rt. The crude product was purified by reprecipitation from diethyl ether and extracted with distilled water. The H12–PEG–Glu2C18 was obtained as a white solid (63 mg, 12 μmol, 47%).

Physicochemical Properties of H12–PEG–Glu2C18. TLC (silica gel, chloroform/methanol = 4/1, v/v): R_f 0.17. IR (film; cm^{-1}): 1736($\nu_{C=O}$, ester). ^1H NMR ($CDCl_3$, 500 MHz, δ ppm): 0.89 (t, 6H, $-CH_3$), 1.26 (br, 60H, $-CH_2-$), 1.63 (m, 4H, $-COOCH_2CH_2-$), 2.00 (m, 2H, $-CH_2CHCON-$), 2.46 (m, 2H, $-CH_2COO-$), 4.08 (m, 4H, $-COOCH_2-$), 3.63 (br, 360H, PEG).

Preparation of H12–PEG–vesicles. DPPC (100 mg, 136 μmol), cholesterol (52.7 mg, 136 μmol), DHSG (18.9

mg, 27.2 μmol), PEG–DSPE (5.2 mg, 0.90 μmol), and H12–PEG–Glu2C18 (0, 0.47, 1.57, 4.7, or 9.4 mg; 0, 0.090, 0.30, 0.90, or 1.8 μmol, respectively) were dissolved in benzene and then freeze-dried. The resulting white powder was hydrated with distilled water and extruded with membrane filters (pore sizes 3.00, 0.80, 0.65, 0.30, or 0.22 μm, FM filter, Fuji Film, Tokyo). The vesicles were washed with phosphate-buffered saline (PBS, pH 7.4) by suspension and centrifugation (100 000*g*, 30 min, 4 °C, twice). The particle diameter was analyzed by a dynamic light scattering method (N4 PLUS, Beckman-Coulter, Fullerton, FL). We prepared PEG–vesicles or vesicles using lipids in the absence of H12–PEG–Glu2C18 or H12–PEG–Glu2C18 and PEG–DSPE, respectively.

Measurement of the Stability of H12–PEG–vesicles. For the measurement of the incorporation ratio of H12–PEG–Glu2C18 to the vesicle, the H12–PEG–vesicles dispersion was freeze-dried to dissolve in $CDCl_3$. The peak area ratio (R_1) of the choline methyl proton of DPPC (3.37 ppm) to the methylene proton of the PEG chain in H12–PEG–Glu2C18 (3.64 ppm) was measured by ^1H NMR spectroscopy (JNM-Lambda 500, JEOL, Tokyo) to determine the incorporation ratio of the H12–PEG–Glu2C18. To study the change of the incorporated PEG lipids in the vesicles, the 30-fold diluted sample dispersion ([lipid] = 0.58 M in PBS, pH 7.4) was incubated at 37 °C, and R_1 was calculated from the ^1H NMR spectrum as described above. The peak area ratio before the incubation was defined as R_0. The incorporation ratio was calculated from a percentage of R_1 to R_0.

Preparation of Collagen Immobilized on a Surface. Collagen I-A (3.0 mg/mL) was suspended in PBS at 4 °C (30 μg/mL), and glass plates (diameter 24 mm, thickness 0.5 mm) were immersed into the collagen suspension at 4 °C for 8 h. The glass plates were carefully rinsed with PBS and immersed in a bovine serum albumin solution (20 mg/mL) at rt for 2 h before perfusion studies were performed, as described below.

Preparation of Platelets Immobilized on a Surface. Blood withdrawn from three healthy volunteers was mixed with a 10% volume of 3.8% (w/v) sodium citrate. Platelet-rich plasma (PRP) was prepared by centrifugation (100*g*, 15 min, 22 °C). The PRP was mixed with a 15% volume of acid–citrate–dextrose composed of 2.2% (w/v) sodium citrate, 0.8% (w/v) citric acid, and 2.2% (w/v) glucose (ACD) containing 1 μM prostaglandin E_1 (PGE_1, Sigma, St. Louis, MO). The suspension was centrifuged (2200*g*, 10 min, 22 °C), and the plasma was replaced with a Ringer's–citrate–dextrose solution (RCD solution, composition 0.76% (w/v) citric acid, 0.090% (w/v) glucose, 0.043% (w/v) $MgCl_2$, 0.038% (w/v) KCl, 0.60% (w/v) NaCl, pH 6.5) containing 1 μM PGE_1. After the pellets were resuspended in the RCD solution, the suspension was centrifuged (2200*g*, 10 min, 22 °C), and the concentrated platelets were resuspended at $2.0 \times 10^5/\mu L$ in a Hepes–Tyrode buffer (H–T buffer, pH 7.4). The platelet counts were determined using an automated hematology analyzer (K-4500, Sysmex, Kobe, Japan). A collagen-coated glass plate was immersed into the platelet suspension for 1 h at 37 °C and carefully rinsed with PBS.

Measurement of Interaction of the H12–PEG–vesicles with Platelets Immobilized on a Glass Plate using Reconstituted Blood. Blood containing a 10% volume of 3.8% (w/v) sodium citrate was centrifuged (100*g*, 15 min, 22 °C) to replace PRP with an equal volume of a 0.9% (w/v) NaCl solution containing 10% (v/v) ACD (10% ACD–saline). The red blood cell suspension was centrifuged (2200*g*, 10 min, 22 °C) and washed with 10% ACD–saline three times to remove the buffy coat and plasma completely. After the final centrifugation, the red blood cells were resuspended in a H–T buffer to adjust the hematocrit (Hct) to 50%. The residual platelet counts were determined to be $(5.0 \pm 2.0) \times 10^3/\mu L$.

A solution of $DiOC_{18}$ in DMSO (10 mM, 50 μL) was added to the H12–PEG–vesicle suspension (20 mg/mL, 5 mL), and the suspension was incubated at rt for 30 min. The free $DiOC_{18}$ was separated by washing with PBS and centrifugation at 100 000*g* for 30 min at 4 °C twice, and the $DiOC_{18}$-labeled H12–PEG–vesicles were collected.

The reconstituted blood and the $DiOC_{18}$-labeled H12–PEG–vesicle mixtures were placed in a recirculating chamber mounted on an epifluorescent microscope (ECLIPS TE300, Nikon, Tokyo) equipped with a CCD camera, and the interaction of the H12–PEG–vesicles with the platelets immobilized on the surface was observed. All perfusion studies were performed at 37 °C. Single-frame images of the H12–PEG–vesicles on the plates were obtained with an image processor, Argus-50 (Hamamatsu Photonics, Hamamatsu).

Measurement of the Dynamic Interaction of Platelets in Thrombocytopenia-Imitation Blood with a Collagen-Coated Surface in the Presence of the H12–PEG–vesicles. Blood containing PPACK (40 μM), a thrombin inhibitor, was filtered with a leukocyte removal filter (NEO1J, Nihon Poll, Tokyo), which can remove both leukocytes and platelets from whole blood. The residual platelet count in the blood was $(6.0 \pm 2.0) \times 10^3/\mu L$. The platelet count was adjusted to $5.0 \times 10^4/\mu L$ with PRP. This blood preparation was termed thrombocytopenia-imitation blood.

Platelets in the blood were labeled with $DiOC_6$ (final concentration, 2 μM), and the H12–PEG–vesicles were added to the blood for 5 min at 37 °C ([lipid] = 0.89 mM). The blood was placed in a recirculating chamber mounted on an epifluorescent microscope as described above, and the interaction of platelets with the collagen immobilized on the surface was observed. The surface coverage of the platelets that adhered on the plate was calculated with an image processor, Argus-20 (Hamamatsu Photonics).

Measurement of PAC-1 Binding and P-Selectin Expression of Resting Platelets in the Presence of the H12–PEG–vesicles Using Flow Cytometry. H12–PEG–vesicles or PEG–vesicles (final lipid concentration 0.82 μM) were added to PRP ([platelet] = $5.0 \times 10^4/\mu L$), and the mixtures were stirred at 37 °C for 30 min. Before and after stirring, FITC-labeled anti-P-selectin antibody (approximately 0.5 μg) was added to the mixture, incubated at 37 °C for 10 min, and then fixed with formaldehyde (final concentration 1.5% (v/v)). Alternatively, FITC-labeled PAC-1 (approximately 0.5 μg) was added to the mixture of platelets and samples and stirred at 37 °C for 10 min, followed by fixing with formaldehyde. As a positive control, ADP-stimulated platelets (final concentration of ADP; 20 or 100 μM) were prepared from PRP. The platelets were gated according to their characteristic forward versus side scatter, and 20 000 platelets were analyzed using a FACSCalibur flow cytometer (Nihon Becton Dickinson, Tokyo). PAC-1 binding or P-selectin expression was quantified as a fraction of the fluorescent-positive platelets. Each experiment was performed at least three times.

Measurement of Tail Bleeding Time and Half-Life of H12–PEG–vesicles Using Thrombocytopenic Rats. All animal studies were approved by the Animal Subject Committee of Keio University School of Medicine and performed according to NIH guidelines for the care

and use of laboratory animals. Experiments were carried out using male Wistar rats (230–250 g, CLEA Japan, Tokyo). A busulfan solution was prepared at a final concentration of 5 mg/mL in poly(ethylene glycol) (average molecular weight 400) (*11*, *43*, *44*). Rats were anesthetized with diethyl ether and injected on day 0 and day 3 with 10 mg/kg on each dosing day to produce a total dosage of 20 mg/kg of busulfan. On day 10, thrombocytopenic rats were anesthetized with sevofrane, and the sample suspension was infused into the tail vein. The samples were the H12–PEG–vesicles and the PEG–vesicles at a dose of 4 mL/kg; saline was used for control. Five minutes after administration, a template-guided incision (Quikheel, Becton-Dickinson, San Jose, CA) 2.5 mm in length and 1.0 mm in depth was made 1 cm from the tip of the tail. The tail was immersed in a 50 mL cylinder of saline, and the time taken for bleeding to stop was measured. In addition, blood was sampled from ether-anesthetized rats 5 min before and 30 min after sample injection by inserting a 25-gauge needle into the tail vein, and the cell counts were determined using an automated hematology analyzer (K-4500).

Half-life was measured from the β-phase of the clearance curve as follows: the $DiOC_{18}$-labeled H12–PEG–vesicles, PEG–vesicles, or vesicles were infused into the tail vein of thrombocytopenic rats at a dose of 40 mg/kg (equivalent lipid concentration). Following this, 400 μL of blood was collected from the tail vein of the rats at time intervals and centrifuged (2200*g*, 10 min, 22 °C), and 200 μL of plasma containing vesicles was collected. The plasma was mixed with deca(oxyethylene) dodecyl ether ($C_{12}E_{10}$) and was heated at 42 °C for 2 min to enhance the solubilization of the vesicles. The fluorescent intensity was then measured (E_x = 485 nm, E_m = 500 nm), and the half-life was calculated using a spectrofluorometer (FP-750, JASCO, Tokyo).

Statistical Analysis. Statistical significance of the results for H12–PEG–vesicles group vs the PEG–vesicles group was tested with Tukey–Kramer tests (Figure 4). A P value of less than 0.05 was considered to be statistically significant. Statistical analyses were performed using Stat View software (SAS Institute).

RESULTS

Characterization of H12–PEG–vesicles. L-Glutamic acid was selected as a connector to synthesize PEG–lipid derivatives as shown in Scheme 1. Each of the two carboxyl groups of the glutamic acid were bonded to a stearyl alcohol molecule by an ester bond to produce a hydrophobic moiety. The product, Glu2C18, was obtained after reprecipitation and recrystallization with a yield of 80%. MAL–PEG–Glu2C18 was obtained from the reaction of MAL–PEG–NHS and Glu2C18 with a yield of 64%. Cys-H12, where cysteine was introduced at the N terminal end of H12, was reacted with MAL–PEG–Glu2C18 in DMF to obtain H12–PEG–Glu2C18. In the ^{1}H NMR spectrum of H12–PEG–Glu2C18, the peak (δ = 6.70 ppm) that was attributed to the maleimide group of MAL–PEG–Glu2C18 disappeared, indicating the bonding of the thiol group of the cysteine with the maleimide group of MAL–PEG–Glu2C18 (yield 47%).

Next, we prepared H12–PEG–vesicles (220 ± 70 nm), DPPC/cholesterol/DHSG = 5/5/1, by molar ratio (Figure 1), which were modified with PEG–DSPE (0.3 mol %) and H12–PEG–Glu2C18 (from 0.03 to 0.6 mol %). The molecular weights of the PEG chain of the PEG–DSPE and H12–PEG–Glu2C18 were 5.0 and 3.1 kDa, respectively. The incorporated ratio (R_1/R_0) of the H12–PEG–Glu2C18 (0.3 and 0.6 mol %) was measured after incubation at 37 °C in a 30-fold dilution to analyze the stability of the lipids in the vesicle. From the ^{1}H NMR analyses, the R_1/R_0 of the H12–PEG–Glu2C18 did not change after the incubation for 12 h at 37 °C. The endotoxin concentration in the H12–PEG–vesicle suspension ([lipid] = 53.5 mM) was below 0.2 EU/mL. Furthermore, the half-life of H12–PEG–vesicles was estimated to be 200 ± 23 min from the β-phase of the clearance curve. In the cases of the control PEG–vesicles and the bare vesicles, the half-life was calculated to be 268 ± 2 min and 29 ± 1 min, respectively.

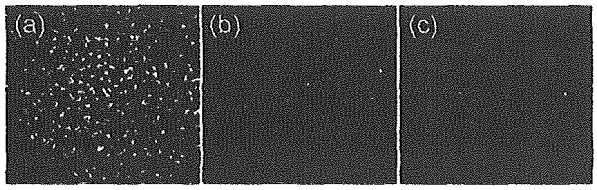

Figure 2. *Specific adhesion* of H12–PEG–vesicles in the reconstituted blood (Hct. 50%, platelet counts = (5.0 ± 2.0) × $10^8/\mu$L) to platelets activated on the collagen surface at a shear rate of 150 s^{-1}: (a) H12–PEG–vesicles; (b) H12–PEG–vesicles in the presence of PAC-1; (c) PEG–vesicles. Images a–c were obtained after blood was circulated for 500 s ([lipid] = 0.89 M).

Interaction of the H12–PEG–vesicles with Platelets Immobilized on a Surface under Flow Conditions. $DiOC_{18}$-prelabeled H12–PEG–vesicles (modification ratio of H12 0.3 mol %) were mixed with the reconstituted blood, and the mixture was allowed to flow over the activated platelets that were adhering to the collagen surface at a shear rate of 150 s^{-1}. The vesicles adhered and accumulated on the surface in a time-dependent manner, whereas the control PEG–vesicles did not adhere (Figure 2). The adhesion of the H12–PEG–vesicles was suppressed in the presence of PAC-1, an inhibitor of GPIIb/IIIa of the activated platelets.

Platelet Adhesion to a Collagen-Coated Surface in Thrombocytopenia-Imitation Blood Containing the H12–PEG–vesicles. We prepared a thrombocytopenia-imitation blood and adjusted the platelet counts to 5.0 × $10^4/\mu$L. The platelets were labeled with a fluorescent reagent, $DiOC_6$, to observe the dynamic interactions of the platelets with the collagen-coated surface at a shear rate of 150 s^{-1}. In this case, vesicles were not labeled. In the presence of the control PEG–vesicles, the surface coverage of platelets gradually increased to 10.6% ± 1.3% after 300 s of flow (Figure 3A, filled triangle). The value was not appreciably different (9.1% ± 0.4%) in the absence of the PEG–vesicles (Figure 3A, filled circle). When the H12–PEG–vesicles (modification ratio of H12 0.3 mol %) were added to the blood in the same way, the initial adhesion rate was comparable to that obtained with the PEG–vesicles; however, the adhesion rate increased dramatically with time, and the surface coverage reached 17.2% ± 1.9% (Figure 3A, opened circle).

We carried out the same experiments using the H12–PEG–vesicles with various modification ratios of the H12–PEG–Glu2C18 from 0 to 0.6 mol % (Figure 3B). The surface coverage of the PEG–vesicles and the H12–PEG–vesicles having the modification ratio of 0.1 mol % was 8.8% ± 1.8% and 9.5% ± 4.2% after 300 s of flow, respectively. When the H12-modification ratio was higher than 0.3 mol %, the surface coverage increased significantly to 17.2% ± 1.9% and then saturated.

PAC-1 Binding to and P-Selectin Expression of Platelets in the Presence of the H12–PEG–vesicles.

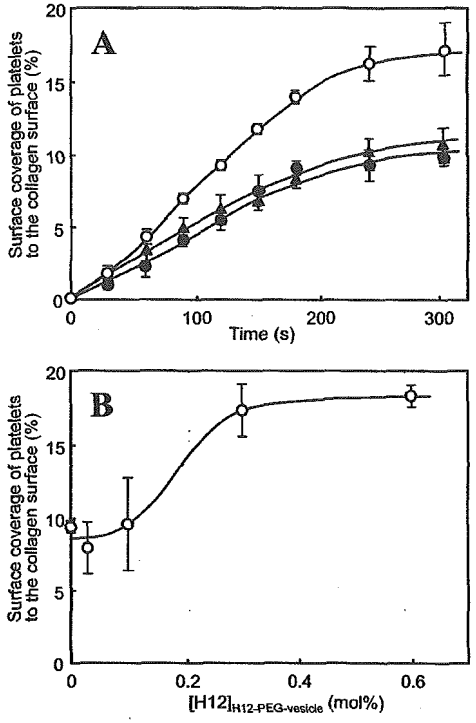

Figure 3. (A) Time course studies of surface coverage of platelets in the thrombocytopenic-imitation blood on the collagen surface after addition of (○) H12–PEG–vesicles, (●) PEG–vesicles, and (▲) PBS and (B) comparison between surface coverage of platelets and modification ratio of H12 on the surface of vesicles (shear rate 150 s^{-1}, [platelets] = 5.0 × $10^4/\mu L$, [lipid] = 0.89 M, N = 3). The surface coverage was measured after 300 s.

Table 1. Binding Ratios of PAC-1 and Anti-P-selectin Antibody to the Resting Platelets in the Presence of H12–PEG–vesicles (N = 3)

stirring time (min)	PAC-1 binding (%)		P-selectin expression (%)	
	0	10	0	10
PBS	0.37 ± 0.12	3.77 ± 0.89	0.35 ± 0.11	2.52 ± 0.52
PEG–vesicles	0.52 ± 0.11	3.35 ± 0.32	0.50 ± 0.09	2.27 ± 0.54
H12–PEG–vesicles ([H12] = 0.3 mol %)	0.34 ± 0.16	3.72 ± 0.53	0.40 ± 0.10	2.43 ± 0.21
	89.80 ± 10.90[a]		33.42 ± 6.87[b]	

[a] ADP = 100 μM. [b] ADP = 20 μM.

We measured the ratios of PAC-1 binding to platelets and the P-selectin expression of platelets in the presence of the H12–PEG–vesicles (modification ratio of H12 0.3 mol %) (Table 1). In the ADP-stimulated and the resting platelets, the PAC-1 binding ratio was 89.8% ± 10.9%, and 0.37% ± 0.12%, respectively. When the resting platelets were stirred for 10 min at 37 °C, the ratio increased slightly to 3.77% ± 0.89%. Before and after mixing with the H12–PEG–vesicles, the ratio was 0.34% ± 0.16% and 3.72% ± 0.53%, respectively. In the case of the PEG–vesicles, the values (before 0.52% ± 0.11%, after 3.35% ± 0.32%) were approximately the same as those of the H12–PEG–vesicles.

On the other hand, the P-selectin expression ratios before and after mixing with the H12–PEG–vesicles were 0.40% ± 0.10% and 2.43% ± 0.21%, respectively, whereas in the PEG–vesicles, the values did not change (before 0.50% ± 0.09%, after 2.27% ± 0.54%). The positive and negative controls were 33.42% ± 6.87% and 0.35% ± 0.11%, respectively.

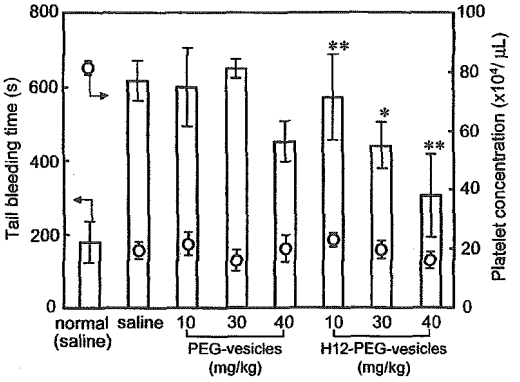

Figure 4. Effects of the administration of H12–PEG–vesicles on tail bleeding time. The administered amount of H12–PEG–vesicles was 10, 30, or 40 mg/kg equivalent of lipid. ○ indicates the platelet concentration in the rats (N = 6–10); * indicates P < 0.05 or ** indicates not significant for H12–PEG–vesicles vs PEG–vesicles group at the same dose.

Measurement of the Tail Bleeding Time of Thrombocytopenic Rats in the Presence of the H12–PEG–vesicles. Thrombocytopenic rats were prepared by administering busulfan at a total dose of 20 mg/kg as described in our previous study (*11*). The tail bleeding times of normal rats ([platelet] = (8.1 ± 0.9) × $10^5/\mu L$) and thrombocytopenic rats ([platelet] = (2.0 ± 0.3) × $10^5/\mu L$) were 178 ± 56 and 618 ± 51 s, respectively (Figure 4). The bleeding time of the thrombocytopenic rats was about 3.5 times longer than that of the normal rats. Intravenous administration of the H12–PEG–vesicles at a dose of 10 mg/kg slightly reduced the bleeding time to 573 ± 127 s in comparison with those of a saline group (618 ± 51 s) or a control PEG–vesicle group at the same dose of the H12–PEG–vesicles (598 ± 115 s). At doses of 30 and 40 mg/kg, we confirmed a dose-dependent reduction of the bleeding time as shown in Figure 4; the time decreased significantly to 441 ± 66 and 335 ± 96 s, respectively. By comparison, the bleeding times of the control PEG–vesicles groups at doses of 30 and 40 mg/kg were 662 ± 21 and 432 ± 22 s, respectively. At the dose of 30 mg/kg, H12–PEG–vesicles significantly reduced the bleeding time in comparison with controls, whereas the H12–PEG–vesicles tended to reduce the bleeding time at the dose of 40 mg/kg.

DISCUSSION

We previously showed that fibrinogen-related dodecapeptide (H12) did not interact with the nonactivated platelets and did not cause platelet activation by using H12-latex beads (*34*). This indicated that H12 is a promising candidate as a key material of platelet substitutes. In this paper, we prepared H12–vesicles modified with PEG to obtain information about the possibility of constructing biocompatible and biodegradable particles with hemostatic ability in thrombocytopenic conditions. On the other hand, PEG-conjugated phosphatidylethanolamines (PEG–phospholipids) have been widely used for modification of the surface of vesicles to prolong the blood circulation time or to stabilize their dispersion states (*40–44*). Furthermore, PEG–phospholipids in which the terminus has an active group such as maleimido and pyridyl disulfide groups were also utilized to conjugate receptor proteins or ligands. We are proposing the use of amino acid-based lipids instead of phospholipid because various modifications are possible by simple syntheses. In this study, we used the PEG-conjugated amino acid-based lipid, as in our previous studies (*41*,

42). L-Glutamic acid was used as a connector between the PEG chain and two hydrophobic chains, in this case, stearyl alcohol (Glu2C18). The length of the alkyl chain is important because shorter alkyl chains should result in the dissociation of the PEG–lipid from the surface of the vesicle. The amino group of Glu2C18 reacted with the NHS group of MAL–PEG–NHS to produce MAL–PEG–Glu2C18 with a yield of 64%. The low yield is understandable because the NHS group was degraded before or during the reaction by hydrolysis. H12–PEG–Glu2C18 was thus obtained in a relatively high yield via an addition reaction between the maleimido and the mercapto groups of H12.

Next, we prepared vesicles consisting of DPPC/cholesterol/DHSG/PEG–DSPE at a molar ratio of 5/5/1/0.033. The vesicles with this composition were confirmed to be very stable in the state of aqueous dispersion and had excellent blood compatibility with an adequate blood circulation time (41). In the case of the PEG modification ratio of 0.3 mol %, the PEG chain is considered to take a so-called mushroom structure on the surface of the vesicle (45). For example, if 0.3 mol % of PEG–DSPE (M_w 5.0 kDa) and 0.3 mol % of H12–PEG–Glu2C18 (M_w of PEG chain 3.4 kDa) were incorporated in the surface of the vesicle, the excluded volume of the PEG chains would be estimated from the globular polymer chain as a radius of 6.2 and 4.9 nm, respectively, and the linear dodecapeptide (ca. 4.5 nm) was conjugated to the end of the PEG chain. This means that the H12 should locate on the more outer side more than the neighboring PEG chains, and therefore, the H12 has a possibility to be recognized by the platelets activated on the collagen plate.

The H12–PEG–Glu2C18 was incorporated into the bilayer membrane of the H12–PEG–vesicles in an equilibrium state. We have to determine whether the PEG–lipid tends to dissociate from the vesicular surface after dilution of the H12–PEG–vesicle suspension. We measured the incorporated ratio of H12–PEG–Glu2C18 (0.3 and 0.6 mol %) after incubation at 37 °C in a 30-fold dilution to analyze the stability of the lipids incorporated in the vesicles. From the ^{1}H NMR analyses, the incorporated ratio of the H12–PEG–Glu2C18 did not change. This indicated that the H12–PEG–Glu2C18 with the molecular weight of 4.4 kDa could be tethered to the vesicular surface with two stearoyl chains of Glu2C18. Therefore, the H12–PEG–vesicles would circulate stably in vivo without dissociation of the PEG–lipids. Furthermore, we confirmed that the half-life of the H12–PEG–vesicles was approximately 7-fold longer than that of the bare vesicles due to the effect of PEG modification, indicating that the H12–PEG–vesicles were useful for prophylactic transfusion. We are now studying the prolongation of the hemostatic effects at 180 min and longer after the intravenous administration of the H12–PEG–vesicles.

We prepared the immobilized-platelet surface and reconstituted blood to determine whether the H12–PEG–vesicles specifically bind to the immobilized platelets. In our previous studies, the flowing platelets specifically tethered and adhered to the platelets immobilized on the collagen plate, and the adhesion was suppressed in the presence of PAC-1 (46), soluble RGD, or soluble H12, which are GPIIb/IIIa antibodies or inhibitors, indicating that the immobilized-platelet plate should have GPIIb/IIIa exposed on the surface (9, 47) (data not shown). Especially, PAC-1 recognizes an epitope on the GPIIb/IIIa complex of activated platelets at or near the platelet fibrinogen receptor (46). In reconstituted blood flowing over the immobilized-platelet plate, the H12–PEG–vesicles adhered and accumulated on the surface, whereas the control PEG–vesicles did not adhere as shown in Figure 2. When PAC-1 was added to the blood containing the H12–PEG–vesicles, the adhesion of the H12–PEG–vesicles was completely inhibited, indicating that the H12–PEG–vesicles were specifically bound to the activated GPIIb/IIIa on the surface of the platelets even with PEG modification. This was supported by the results showing that the number of the adherent H12–PEG–vesicles increased with increasing H12-modification ratio to the vesicle from 0.03 to 0.6 mol % (data not shown).

To determine whether the H12–PEG–vesicles have an ability to reinforce thrombus formation under thrombocytopenic conditions, we prepared a thrombocytopenic blood and adjusted the number of platelets to $5.0 \times 10^4/\mu L$ (one-fifth of normal). When the thrombocytopenic blood flowed over the collagen surface, the control PEG–vesicles did not influence the surface coverage of platelets as shown in Figure 3A (filled circle). In the case of the H12–PEG–vesicles having 0.3 mol % H12, the enhancement of the platelet thrombus formation was confirmed as shown in Figure 3A (opened circle). These results suggest that the H12–PEG–vesicles cross-link the activated platelets to enhance the platelet aggregation. In the initial 30 s, the adhesion rate of platelets in the presence of the H12–PEG–vesicles was similar to that of the PEG–vesicles, and then the surface coverage increased dramatically with time in the case of the H12–PEG–vesicles. Furthermore, we confirmed that the H12–PEG–vesicles labeled with rhodamine were involved in the platelet thrombus labeled with $DiOC_6$ by a double-stain method (data not shown). The above results suggest that (1) the adhesion of the H12–PEG–vesicles could be initiated by the activated platelets, which had already adhered on the surface of the immobilized-collagen plate, (2) the H12–PEG–vesicles adhering to the surface of the platelet could act as binding sites for the activated platelets, and (3) the H12–PEG–vesicles could accelerate the formation of the thrombus of the remaining flowing platelets in the thrombocytopenic blood.

Figure 3B summarized the results of the surface coverage of platelets after 300 s in the presence of the H12–PEG–vesicles in which the modification ratio of H12 is from 0 to 0.6 mol % in thrombocytopenic blood. From 0 to 0.1 mol %, the constant surface coverage in the region of the modification ratios suggests that the recognition ability of the H12–PEG–vesicles to the GPIIb/IIIa on the activated platelets was very low because of the low modification density of H12. Surprisingly, the surface coverage increased significantly when the modification ratio was raised above 0.3 mol %. This indicated that the H12–PEG–vesicles had the ability to cross-link the activated platelets. Therefore, we adopted the H12 modification ratio of 0.3 mol %.

Before in vivo studies, we used platelet-activation markers, PAC-1 or anti-P-selectin antibody (48), to determine whether the H12–PEG–vesicles caused the activation of platelets. P-selectin is a membrane glycoprotein existing in the α granules of platelets and Weibel–Palade bodies of vascular endothelial cells, and following cellular activation, it becomes surface-expressed by exocytosis (48). When a mixture of platelets and the control PEG–vesicles was stirred with PAC-1 or anti-P-selectin antibody, the binding ratios of both antibodies to the platelets were slightly increased after stirring as shown in Table 1. These phenomena were also observed in the absence of the control PEG–vesicles or in the

presence of H12–PEG–vesicles as shown in Table 1. This suggested that the increase was caused by stirring and was within the error limit in comparison with that of PAC-1 binding and P-selectin expression to ADP-stimulated platelets. We concluded that the H12–PEG–vesicles did not activate platelets and did not interact with the nonactivated platelets under flow and that the adhesion of the H12–PEG–vesicles was induced by the platelets activated by the collagen surface. Therefore, H12–PEG–vesicles have the potential to be a candidate for platelet substitutes.

Next, we evaluated the hemostatic ability of the H12–PEG–vesicles using thrombocytopenic rats. In our previous studies, we succeeded in preparing thrombocytopenic rats by busulfan administration and getting the extinction curve of platelets reproducibly (*11*). From the data of hematologic indices, where the platelet counts were sufficiently decreased and the erythrocyte and leukocyte counts were maintained, we determined that the appropriate total dosage of busulfan for the rats (8 weeks) was 20 mg/kg. The incision of the tail was to be made on Day 10 after busulfan infusion. We also confirmed that the bleeding time correlated with their platelet concentration, indicating that the tail bleeding time was an effective evaluation parameter for measuring the hemostatic capability of the platelet substitutes.

As shown in Figure 4, the bleeding time of the thrombocytopenic rats was significantly extended in comparison with that of normal rats 5 min after the intravenous administration of saline, and we determined that it was possible to evaluate the hemostatic effect of the H12–PEG–vesicles in vivo using thrombocytopenic rats. The circulating H12–PEG–vesicles at the dose of 30 mg/kg significantly reduced the bleeding time of the thrombocytopenic rats, whereas at a lower concentration of 10 mg/kg, the hemostatic effect did not reach a significant level. At a higher concentration of 40 mg/kg, however, the bleeding time was significantly reduced in comparison with that of the saline group but not with the control PEG–vesicles group (40 mg/kg). This suggested that the PEG–vesicles themselves possessed a hemostatic activity at the higher concentration, because the PEG–vesicles having negative charge at pH 7.4 might nonspecifically bind to site of bleeding injury.

We estimated that the hemostatic ability of the H12–PEG–vesicles at a dose of 30 mg/kg (approximately 2.0×10^{12} particles) would correspond to 1/500th of the hemostatic ability in particle base, which was based on the bleeding time of the thrombocytopenic rats and platelet concentration. Furthermore, we confirmed that hematologic indices such as the platelet and leukocyte counts did not change before and after the administration of the H12–PEG–vesicles.

In conclusion, we demonstrated that the H12–PEG–vesicles did not interact with nonactivated platelets, and the vesicles were shown to preferentially interact with an activated platelet surface via GPIIb/IIIa receptors and to facilitate platelet accumulation at sites of hemostasis. Furthermore, the H12–PEG–vesicles could reduce the tail bleeding time of thrombocytopenic rats. Thus, the H12–PEG–vesicles may be a suitable candidate for an alternative to human platelet concentrates infused into thrombocytopenic patients.

ACKNOWLEDGMENT

The authors thank Drs. M. Murata and K. Yokoyama at Keio University for useful discussion about the functional evaluation of H12 peptide. This work was supported in part by Health and Labor Sciences Research Grants (Research on Pharmaceutical and Medical Safety, S.T., M.H., and Y.I.), Ministry of Health, Labor and Welfare, Japan, and grants-in-aid from the JSPS, Japan (No. 15300171, S.T.), Ministry of Education, Culture, Sports, Science and Technology (Leading Project for Biosimulation, M.H.), 21COE "Practical Nano-Chemistry", and "Consolidated Research Institute for Advanced Science and Medical Care" from MEXT (S.T.), Japan. Y.O. was the recipient of a Research Fellowship from the JSPS for Young Scientists.

LITERATURE CITED

(1) Blajchman, M. A. (2003) Substitutes and alternatives to platelet transfusions in thrombocytopenic patients. *J. Thromb. Haemostasis 1*, 1637–1641.

(2) Rybak, M., and Renzulli, L. A. (1993) A liposome based platelet substitutes, the plateletsome, with hemostatic efficacy. *Biomater. Artif. Cells Immobilization Biotechnol. 21*, 108–118.

(3) Graham, S. S., Gonchoroff, N. J., and Miller, J. L. (2001) Infusible platelet membranes retain partial functionality of the platelet GPIb/IX/V receptor complex. *Am. J. Clin. Pathol. 115*, 144–147.

(4) Levi, M., Friedrich, P. W., Middleton, S., De Groot, P. G., Wu, Y. P., Harris, R., Biemond, B. J., Heijien, F. G., Levin, J., and Ten Cate, J. W. (1999) Fibrinogen-coated albumin microcapsules reduce bleeding in severely thrombocytopenic rabbits. *Nat. Med. 5*, 107–111.

(5) Agam, G., and Livine, A. A. (1992) Erythrocytes with covalently bound fibrinogen as a cellular replacement for the treatment of thrombocytopenia. *Eur. J. Clin. Invest. 22*, 105–112.

(6) Casals, E., Verdaguer, A., Tonda, R., Galan, A., Escolar, G., and Estelrich, J. (2003) Atomic force microscopy of liposomes bearing fibrinogen. *Bioconjugate Chem. 14*, 593–600.

(7) Coller, B. S., Springer, K. T., Beer, J. H., Mohandas, N., Scudder, L. E., Norton, K. J., and West, S. M. (1992) Thromboerythrocytes. In vitro studies of a potential autologous, semi-artificial alternative to platelet transfusion. *J. Clin. Invest. 89*, 546–555.

(8) Teramura, Y., Okamura, Y., Takeoka, S., Tsuchiyama, H., Narumi, H., Kainoh, M., Handa, M., Ikeda, Y., and Tsuchida, E. (2003) Hemostatic effects of polymerized albumin particles bearing rGPIa/IIa in thrombocytopenic mice. *Biochem. Biophys. Res. Commun. 306*, 256–260.

(9) Takeoka, S., Teramura, Y., Okamura, Y., Handa, M., Ikeda, Y., and Tsuchida, E. (2001) Fibrinogen-conjugated albumin polymers and their interaction with platelets under flow conditions. *Biomacromolecules 2*, 1192–1197.

(10) Takeoka, S., Teramura, Y., Ohkawa, H., Ikeda, Y., and Tsuchida, E. (2000) Conjugation of von Willebrand factor-binding domain of platelet glycoprotein Ibα to size-controlled albumin microsheres. *Biomacromolecules 1*, 290–295.

(11) Okamura, Y., Takeoka, S., Teramura, Y., Maruyama, H., Tsuchida, E., Handa, M., and Ikeda, Y. (2005) Hemostatic effects of fibrinogen-γ chain dodecapeptide-conjugated polymerized albumin particles *in vitro* and *in vivo*. *Transfusion 45*, 1221–1228.

(12) Takeoka, S., Teramura, Y., Okamura, Y., Tsuchida, E., Handa, M., and Ikeda, Y. (2002) Rolling properties of rGPIbα-conjugated phospholipid vesicles with different membrane flexibilities on vWf surface under flow conditions. *Biochem. Biophys. Res. Commun. 296*, 765–770.

(13) Kitaguchi, T., Murata, M., Iijima, K., Kamide, K., Imagawa, T., and Ikeda, Y. (1999) Characterization of liposomes carrying von Willebrand factor-binding domain of platelet glycoprotein Ibα: A potential substitute for platelet transfusion. *Biochem. Biophys. Res. Commun. 261*, 784–789.

(14) Nishiya, T., Murata, M., Handa, M., and Ikeda, Y. (2000) Targetting of liposomes carrying recombinant fragments of platelet membrane glycoprotein Ibα to immobilized von Willebrand factor under flow conditions. *Biochem. Biophys. Res. Commun. 270*, 755–760.

(15) Nishiya, T., Kainoh, M., Murata, M., Handa, M., and Ikeda, Y. (2002) Reconstitution of adhesive properties of human platelets in liposomes carrying both recombinant glycoproteins Ia/IIa and Ibα under flow conditions: specific synergy of receptor−ligand interactions. *Blood 100*, 136−142.
(16) Murata, M., Ware, J., and Ruggeri, Z. M. (1991) Site-directed mutagenesis of a soluble recombinant fragment of platelet glycoprotein Ibα demonstrating negatively charged residues involved in von Willebrand factor binding. *J. Biol. Chem. 266*, 15474−15480.
(17) Marchese, P., Saldivar, E., Ware, J., and Ruggeri, Z. M. (1999) Adhesive properties of the isolated amino-terminal domain of platelet glycoprotein Ibα in a flow field. *Proc. Natl. Acad. Sci. U.S.A. 96*, 7837−7842.
(18) Sixma, J. J., van Zanten, G. H., Huizinga, E. G., van der Plas, R. M., Verkley, M., Wu, Y. P., Gros, P., and de Groot, P. G. (1997) Platelet adhesion to collagen: An update. *Thromb. Haemostasis 78*, 434−438.
(19) Santro, S. A., and Zutter, M. M. (1995) The α2β1integrin: A collagen receptor on platelets and other cells. *Thromb. Haemostasis 74*, 813−821.
(20) Takagi, J., Petre, B. M., Walz, T., and Springer, T. A. (2002) Global comformational rearrangements in integrin extracellular domains in outside-in and inside-out signaling. *Cell 110*, 599−611.
(21) Xiao, T., Takagi, J., Coller, B. S., Wang, J. H., and Springer, T. A. (2004) Structual basis for allostery in integrins and binding to fibrinogen-mimetic therapeutics. *Nature 432*, 59−67.
(22) Shattil, S. J., Hoxie, J. A., Cunningham, M., and Brass, L. F. (1985) Changes in the platelet membrane glycoprotein IIb-IIIa complex during platelet activation. *J. Biol. Chem. 260*, 11107−11114.
(23) Marguerie, G. A., Plow, E. F., and Edgington, T. S. (1979) Human platelets possess an inducible and saturable receptor specific for fibrinogen. *J. Biol. Chem. 254*, 5357−5363.
(24) Ruggeri, Z. M., De Marco, L., and Gatti, L. (1983) Platelets have more than one binding site for von Willebrand factor. *J. Clin. Invest. 72*, 1−12.
(25) Mustard, J. F., Packham, M. A., and Kinlough-Rathbone, R. L. (1978) Fibrinogen and ADP-induced platelet aggregation. *Blood 52*, 453−466.
(26) De Marco, L., Girolami, A., and Zimmerman, T. S. (1986) Von Willebrand factor interaction with the glycoprotein IIb/IIIa complex. *J. Clin. Invest. 77*, 1272−1277.
(27) Hawiger, J., Kloczewiak, M., Bednarek, M. A., and Timmons, S. (1989) Platelet receptor recognition domains on the α chain of human fibrinogen: structure−function analysis. *Biochemistry 28*, 2909−2914.
(28) Kloczewiak, M., Timmons, S., and Hawiger, J. (1982) Localization of a site interacting with human platelet receptor on carboxy-terminal segment of human fibrinogen γ chain. *Biochem. Biophys. Res. Commun. 107*, 181−187.
(29) Wertheimer, E., Shapiro, B., and Fodor-Salomonowicz, I. (1944) Stability of fibrinogen in normal and pathological plasma. *Br. J. Exp. Pathol. 25*, 121−125.
(30) Kloczewiak, M., Timmons, S., Lukas, T. J., and Hawiger, J. (1984) Platelet receptor recognition site on human fibrinogen. Synthesis and structure−function relationship of peptides corresponding to the carboxy-terminal segment of the γ chain. *Biochemistry 23*, 1767−1774.
(31) Kloczewiak, M., Timmons, S., Bednarek, M. A., Sakon, M., and Hawiger, J. (1989) Platelet receptor recognition domain on the γ chain of human fibrinogen and its synthetic peptide analogues. *Biochemistry 28*, 2915−2919.
(32) Lam, S. C., Plow, E. F., Smith, M. A., Andrieux, A., Ryckwaert, J. J., Marguerie, G., and Ginsberg, M. H. (1987) Evidence that arginyl-glycyl-aspartate peptides and γ chain peptides share a common binding site on platelets. *J. Biol. Chem. 262*, 110−115.
(33) Hallahan, D. E., Geng, L., Cmelak, A. J., Chakravathy, A. B., Martin, W., Scarfone, C., and Gonzalez, A. (2001) Targeting drug delivery to radiation-induced neoantigens in tumor microvasculature. *J. Controlled Release 74*, 183−191.
(34) Takeoka, S., Okamura, Y., Teramura, Y., Watanabe, N., Suziki, H., Tsuchida, E., Handa, M., and Ikeda, Y. (2003) Function of fibrinogen γ-chain dodecapeptide-conjugated latex beads under flow. *Biochem. Biophys. Res. Commun. 312*, 773−779.
(35) Nishiya, T., and Toma, C. (2004) Interaction of platelets with liposomes containing dodecapeptide sequence from fibrinogen. *Thromb. Haemostasis 91*, 1158−1167.
(36) Klibanov, A. L., Maruyama, K., Torchilin, V. P., and Huang, L. (1990) Amphipathic poly(ethylene glycol)s effectively prolong the circulation time of liposomes. *FEBS Lett. 268*, 235−237.
(37) Zalipsky, S. (1995) Functionalized poly(ethylene glycol) for preparation of biologically relevant conjugates. *Bioconjugate Chem. 6*, 150−165.
(38) Sakai, H., Takeoka, S., Park, S. I., Kose, T., Nishide, H., Izumi, Y., Yoshizu, A., Kobayashi, K., and Tsuchida, E. (1997) Surface modification of vHemoglobin vesicles with poly (ethylene glycol) and effects on aggregation, viscosity, and blood flow during 90% exchange transfusion in anesthetized rats. *Bioconjugate Chem. 8*, 23−30.
(39) Sakai, H., Tsai, A. G., Kerger, H., Park, S. I., Takeoka, S., Nishide, H., Tsuchida, E., and Intaglietta, M. (1998) Subcutaneous microvascular responses to hemodilution with a red cell substitutes consisting of poly(ethylene glycol)-modified vesicles encapsulating hemoglobin. *J. Biomed. Mater. Res. 40*, 66−78.
(40) Sou, K., Endo, T., Takeoka, S., and Tsuchida, E. (2000) Poly(ethylene glycol)-modification of the phospholipid vesicles by using the spontaneous incorporation of poly(ethylene glycol)-lipid into the vesicles. *Bioconjugate Chem. 11*, 372−379.
(41) Sou, K., Naito, Y., Endo, T., Takeoka, S., and Tsuchida, E. (2003) Effective encapsulation of proteins into size-controlled phospholipid vesicles using freeze−thawing and extrusion. *Bioconjugate Chem. 19*, 1547−1552.
(42) Takeoka, S., Mori, K., Ohkawa, H., Sou, K., and Tsuchida, E. (2000) Synthesis and assembly of poly(ethylene glycol)-lipids with mono-, di-, tetraacyl chains and a poly(ethylene glycol) chain of various molecular weights. *J. Am. Chem. Soc. 122*, 7927−7935.
(43) Yang, C., Li, Y. C., and Kuter, D. J. (1999) The physiological response of thrombopoietin (c-Mpl ligand) to thrombocytopenia in the rat. *Br. J. Haematol. 105*, 478−485.
(44) Stenberg, P. E., Barrie, R. J., Pestina, T. I., Steward, S. A., Arnold, J. T., Murti, A. K., Hutson, N. K., and Jackson, C. A. (1998) Prolonged bleeding time with defective platelet filopodia formation in the wistar furth rat. *Blood 91*, 1599−1608.
(45) Hristova, K., and Needham, D. (1995) Phase Behavior of a Lipid/Polymer−Lipid Mixture in Aqueous Medium. *Macromolecules 28*, 991−1002.
(46) Taub, R., Gould, R. J., Garsky, V. M., Ciccarone, T. M., Hoxie, J., Friedman, P. A., and Shattil, S. J. (1989) A monoclonal antibody aganst the platelet fibrinogen reseptor contains a sequence that mimics a receptor recognition domein receptor. *J. Biol. Chem. 264*, 259−265.
(47) Kulkarni, S., Dopheide, S. M., Yap, C. L., Ravanat, C., Freund, M., Mangin, P., Heel, K. A., Street, A., Harper, I. S., Lanza, F., and Jackson, S. P. (2000) A revised model of platelet aggregation. *J. Clin. Invest. 105*, 783−791.
(48) Lasky, L. A. (1992) Selectin: interpreters of cell-specific carbohydrate information during inflamation. *Science 258*, 964−969.

BC050178G

THE JOURNAL OF BIOLOGICAL CHEMISTRY
Vol. 280, No. 26, Issue of July 1, pp. 24775–24783, 2005
Printed in U.S.A.

Membrane-proximal α/β Stalk Interactions Differentially Regulate Integrin Activation*

Received for publication, August 19, 2004, and in revised form, April 21, 2005
Published, JBC Papers in Press, April 29, 2005, DOI 10.1074/jbc.M409548200

Tetsuji Kamata‡§, Makoto Handa¶, Yukiko Sato‡, Yasuo Ikeda‖, and Sadakazu Aiso‡

From the Departments of ‡Anatomy, ¶Transfusion Medicine and Cell Therapy, and ‖Internal Medicine, Keio University School of Medicine, Tokyo 160-8582, Japan

The affinity of integrin-ligand interaction is regulated extracellularly by divalent cations and intracellularly by inside-out signaling. We report here that the extracellular, membrane-proximal α/β stalk interactions not only regulate cation-induced integrin activation but also play critical roles in propagating inside-out signaling. Two closely related integrins, αIIbβ3 and αVβ3, share high structural homology and bind to similar ligands in an RGD-dependent manner. Despite these structural and functional similarities, they exhibit distinct responses to Mn^{2+}. Although αVβ3 showed robust ligand binding in the presence of Mn^{2+}, αIIbβ3 showed a limited increase but failed to achieve full activation. Swapping α stalk regions between αIIb and αV revealed that the α stalk, but not the ligand-binding head region, was responsible for the difference. A series of αIIb/αV domain-swapping chimeras were constructed to identify the responsible domain. Surprisingly, the minimum component required to render αIIbβ3 susceptible to Mn^{2+} activation was the αV calf-2 domain, which does not contain any divalent cation-binding sites. The calf-2 domain makes interface with β epidermal growth factor 4 and β tail domain in three-dimensional structure. The effect of calf-2 domain swapping was partially reproduced by mutating the specific amino acid residues in the calf-2/epidermal growth factor 4-β tail domain interface. When this interface was constrained by an artificially introduced disulfide bridge, the Mn^{2+}-induced αVβ3-fibrinogen interaction was significantly impaired. Notably, a similar disulfide bridge completely abrogated fibrinogen binding to αIIbβ3 when αIIbβ3 was activated by cytoplasmic tail truncation to mimic inside-out signaling. Thus, disruption/formation of the membrane-proximal α/β stalk interface may act as an on/off switch that triggers integrin-mediated bidirectional signaling.

Integrins are a family of α/β heterodimeric transmembrane cell surface receptors that mediate cell-extracellular matrix and cell-cell interactions. The hallmark of integrin-dependent adhesive interaction is its regulation by intracellular signaling events (inside-out signaling) and by divalent cations. In addition to mediating adhesive interactions, liganded integrins initiate signals inside the cell to modify cell behavior (outside-in signaling) and thus play fundamental roles in numerous biological processes such as differentiation, cell survival, apoptosis, and cell motility (1). Integrin-mediated bidirectional signaling is accompanied by conformational change of the integrin structure. The crystal structure of αVβ3 extracellular domains revealed an unexpected bent conformer distinct from the extended conformer observed under electron microscope (2, 3). High-resolution electron microscopic observation on truncated recombinant αVβ3 has confirmed the presence of both conformers, suggesting that the transition from one conformer to another might take place under physiological conditions (4). However, integrin extension *per se* is not required for the activation, but the swing-out of the β hybrid domain (the transition from "closed" headpiece to "open" headpiece) that accompanies the extension is the critical event (5). Thus, integrin extracellular domains undergo extensive structural rearrangement (so-called "switchblade-like" movement) upon Mn^{2+}/ligand binding. In support, fluorescence resonance energy transfer measurements between α4β1-bound peptide ligand and plasma membrane revealed that such movement actually takes place in living cells (6, 7).

Divalent cations differentially regulate integrin-ligand interaction. Whereas Mn^{2+} and, to a lesser extent, Mg^{2+} have an enhancing effect, Ca^{2+} typically has an inhibitory effect on ligand binding. Biochemical studies have suggested the existence of three classes of cation-binding sites with distinct function and preference for cations (8). The αVβ3 extracellular domains turned out to contain eight cation-binding sites. Five of them are located in the β-propeller and at the junction between the thigh and calf-1 domains of the α subunit. The other three are located in the βA domain of the β subunit. Besides the metal ion-dependent adhesion site (MIDAS), which is essential for ligand binding (9, 10), the βA domain possesses two additional sites designated ADMIDAS (adjacent to MIDAS) and LIMBS (ligand-associated metal binding site), respectively (11). Whereas ADMIDAS is occupied by a cation regardless of the presence of bound ligand, MIDAS and LIMBS have been shown to bind Mn^{2+} only in the presence of bound ligand (3, 11). A recent report by Chen *et al.* (12) suggests that the ADMIDAS is the negative regulatory site for Ca^{2+}, whereas LIMBS is the positive regulatory site for Ca^{2+}. These reports implicate that the cation-binding sites in the βA domain represent the three classes of cation-binding sites described by Mould *et al.* (8), thus they are primarily responsible for integrin affinity regulation by divalent cations. In contrast, the role of the α subunit, particularly the five cation-binding sites, has not been clearly defined.

* This work was supported by a health and labor science research grant for research on regulatory science of pharmaceuticals and medical devices from the Ministry of Health, Labor and Welfare; a grant for leading project for biosimulation from the Ministry of Education, Culture, Sports, Science and Technology; a grant from Keio Gijuku Fukuzawa Memorial Fund for the advancement of education and research (to T. K. and M. H.); a grant-in-aid for scientific research (B); a grant-in-aid for COE research; and a national grant-in-aid for the establishment of high-tech research center in a private university (to S. A.). The costs of publication of this article were defrayed in part by the payment of page charges. This article must therefore be hereby marked "*advertisement*" in accordance with 18 U.S.C. Section 1734 solely to indicate this fact.

§ To whom correspondence should be addressed: Dept. of Anatomy 3S1, Keio University School of Medicine, 35 Shinanomachi, Shinjuku-ku, Tokyo 160-8582, Japan. Tel.: 81-3-3353-1211 (ext. 63571); Fax: 81-3-5360-1524; E-mail: kamata@sc.itc.keio.ac.jp.

Two β3 integrins, αIIbβ3 and αVβ3 ,share high structural homology (13). Both integrins share a common β3 subunit and bind fibrinogen (Fbg),[1] von Willebrand factor, fibronectin, and vitronectin in an RGD-dependent manner. Despite these structural and functional similarities, divalent cations regulate ligand binding differently in these integrins. Kinetic studies have shown that Mn^{2+} supports Fbg binding to both αIIbβ3 and αVβ3, albeit with a relatively slow association rate, whereas Ca^{2+} supports Fbg binding only to αIIbβ3, but not to αVβ3 (14). In agreement, real-time measurements of Fbg binding interaction have shown that Mn^{2+} increased the affinity for Fbg in both integrins by increasing the association rate (4, 15). Consistent with these observations, αVβ3-mediated cell attachment to immobilized Fbg was greatly enhanced by Mn^{2+} but not by Ca^{2+} (14). In contrast, intact αIIbβ3 expressed on the cell surface exhibits different characteristics. First of all, cations including Mn^{2+} are unable to initiate platelet aggregation or induce Fbg binding to platelets, unless platelets are stimulated by agonists. The agonist-stimulated platelet aggregation is also poorly supported by Mn^{2+} (14, 16, 17). These lines of evidence suggest that cation-binding sites in the βA domain do not account for the distinct response to Mn^{2+} in β3 integrins, but rather that the structural difference in the α subunit may be responsible. In this study, we sought to determine the mechanism that regulates Mn^{2+}-induced activation in β3 integrins. We provide evidence that the calf-2 domain, but not the cation-binding sites, in the α subunit plays a critical role in regulating the Mn^{2+}-induced integrin activation. Furthermore, the results suggest that disruption/formation of the membrane-proximal calf-2/epidermal growth factor (EGF)4-β tail domain (βTD) interface may act as an on/off switch that propagates the conformational signals in integrin-mediated bidirectional signaling.

EXPERIMENTAL PROCEDURES

Antibodies and Reagents—Anti-αIIb monoclonal antibody (mAb) PL98DF6 (18) was a generous gift from Drs. J. Ylänne (University of Uppsala, Uppsala, Sweden) and I. Virtanen (University of Helsinki, Helsinki, Finland). Conformation-dependent anti-β3 mAbs anti-LIBS1 and anti-LIBS2 (19) were generous gifts from Dr. Mark H. Ginsberg (University of California, San Diego, CA). Anti-αIIbβ3 complex-specific ligand-mimetic mAb OP-G2 (20) was a kind gift from Dr. Yoshiaki Tomiyama (University of Osaka, Osaka, Japan). The αIIbβ3 complex-specific anti-αIIb mAb P2, anti-β3 mAb SZ21, and anti-αV mAb AMF-7 were purchased from Beckman Coulter (Fullerton, CA). Anti-αIIbβ3 complex-specific activating mAb PT25-2 and non-functional anti-β3 mAb VNR5-2 have been characterized previously (21). Fluorescein isothiocyanate (FITC)- and R-phycoerythrin-conjugated goat anti-mouse polyclonal antibodies were purchased from BIOSOURCE. Synthetic peptide Gly-Arg-Gly-Asp-Ser (GRGDS) was purchased from Peptide Research Institute (Osaka, Japan). FITC was purchased from Sigma-Aldrich. Human Fbg was purchased from Experimental Cell Research (South Bend, IN).

Construction of Mutant αIIb, αV, and β3 cDNA Clones—The full-length cDNAs for integrin αIIb, αV, and β3 subunits (generous gifts from Dr. Joseph C. Loftus, Mayor Clinic, AZ) were cloned into mammalian expression vector pBJ-1 (kindly provided by Dr. Mark Davis, University of California, San Francisco, CA). A SacI site was engineered into the αV cDNA at site homologous to the endogenous SacI site in the αIIb cDNA by site-directed mutagenesis using Transformer Site-Directed Mutagenesis Kit (BD Biosciences). The cDNAs for B/V and V/B chimeras were created by replacing the SacI-BamHI fragment between αIIb and αV. The cDNAs for αIIb/αV domain-swapping chimeras TC1C2, TC1, T, C1, C2, D, C1C2D, TC2D, and TC1D were created using the overlap extension PCR method. The domain boundaries for each chimera were set as shown in Fig. 1*A*. The cDNAs for B/V 753–755, B/V 760–764, B/V 774, B/V 781–783, B/V 787, B/V 899–900, B/V 902–904, and B/V 958–960 mutants were created by site-directed mutagenesis. In these αIIb mutants, the amino acid sequences in each of the indicated regions were replaced by the corresponding αV sequences (^{753}NSF to VSS, ^{760}VVAAE to FLPIP, Asp^{774} to Glu, ^{781}EHT to QHI, His^{787} to Arg, ^{899}QR to KS, ^{902}MTV to ILY, and ^{958}ALE to GIQ, respectively). Likewise, B/V 760, B/V 761, B/V 762, B/V 763, B/V 764, B/V 899, and B/V 900 mutants represent V760F, V761L, A762P, A763I, E764P, Q899K, and R900S mutations, respectively. The cDNAs for B/V 787/899–900 and B/V 787/900 were created from cDNAs for B/V 787 and B/V 899–900 and for B/V 787 and B/V 900, respectively, by replacing the BamHI fragment. The cDNA for B/V 760–764/787/899–900 was created from cDNAs for B/V 760–764 and B/V 787/899–900 by replacing the SacI fragment. The αV D599A, αV E636A, αV S749C, αIIb F755C, β3 D606C, β3 L717tr (β3tr), and αIIb G991tr (αIIbtr) mutants were created by site-directed mutagenesis. The β3 D606C/L717tr double mutant (606tr) was created from β3 D606C and β3 L717tr by replacing the ApaI fragment. The αIIb F755C/G991tr double mutant (755tr) was created from αIIb F755C and αIIb G991tr by replacing the BamHI fragment. The authenticity of the constructs was confirmed by DNA sequencing.

Cell Culture and Transfection—Chinese hamster ovary (CHO)-K1 cells were cultured in Dulbecco's modified Eagle's medium (Invitrogen) supplemented with 10% fetal calf serum (BIOSOURCE), 1% penicillin and streptomycin (Invitrogen), and 1% non-essential amino acids (Sigma-Aldrich) and maintained at 37 °C in a humidified incubator supplemented with 5% CO_2. Fifty μg of αV or αIIb cDNA construct was co-transfected with 50 μg of β3 cDNA construct into CHO-K1 cells by electroporation. After 48 h, the cells were detached and used for assays.

Flow Cytometry—Cells were detached with phosphate-buffered saline containing 3.5 mM EDTA. After washing, cells were incubated with mAbs in modified HEPES-Tyrode buffer (5 mM HEPES, 5 mM glucose, 0.2 mg/ml bovine serum albumin, and 1× Tyrode's solution) supplemented with 1 mM $CaCl_2$ and 1 mM $MgCl_2$ for 30 min at 4 °C. For some experiments, 1 mM GRGDS peptide was included together with mAbs. After washing, cells were incubated with R-phycoerythrin-conjugated $F(ab')_2$ fragment of goat anti-mouse IgG for 30 min at 4 °C. After washing, cells were resuspended in HEPES-buffered saline (10 mM HEPES, 150 mM NaCl, pH 7.4) containing 1 mM $CaCl_2$ and 1 mM $MgCl_2$, and fluorescence was measured on FACSCalibur (BD Biosciences). To compare the binding of conformation-dependent mAbs among cells expressing different αVβ3 mutants, each mAb binding was normalized by the expression of αVβ3. This relative mAb binding was calculated by dividing the mean fluorescent intensity obtained with each anti-LIBS mAb by the mean fluorescent intensity with non-conformation-dependent anti-β3 mAb SZ21.

Fibrinogen Binding Assay—FITC labeling of human Fbg was performed as previously described (22). Briefly, after adjusting the pH of human Fbg at 1 mg/ml in phosphate-buffered saline to 8.5 with 5% Na_2CO_3, 0.01 volume of 10 mg/ml FITC in Me_2SO was added and incubated at room temperature for 10 min. FITC-labeled Fbg was separated from free FITC on a PD-10 column (Amersham Biosciences) equilibrated with HEPES-buffered saline. The concentration and fluorescence/protein ratio of FITC-labeled Fbg was calculated as previously described. Forty-eight h after transfection, cells were detached and incubated with non-functional anti-β3 mAb VNR5-2 followed by a R-phycoerythrin-conjugated $F(ab')_2$ fragment of goat anti-mouse IgG. In some experiments, cells were treated with 10 mM dithiothreitol (DTT) prior to incubation with mAbs as described previously (21). After washing, cells were incubated with FITC-labeled Fbg (200 μg/ml) with or without 1 mM GRGDS peptide in modified HEPES-Tyrode buffer containing 1 mM $CaCl_2$ and 1 mM $MgCl_2$ or 1 mM $MnCl_2$ for 1 h at 4 °C. In some experiments, mAb PT25-2 was included at 10 μg/ml to activate αIIbβ3. After washing, fluorescence was measured on FACSCalibur. The mean Fbg binding (mean fluorescence intensity in FL1 channel) to cell populations expressing high β3 (fluorescence intensity in FL2 channel > 500) was calculated. Background binding in the presence of 1 mM GRGDS peptide was subtracted to obtain specific binding.

RESULTS

Swapping α Stalk Region Switches the Enhancing Effect of Mn^{2+} on Ligand Binding—To locate the structure in the α subunit responsible for the difference in Mn^{2+} activation, we first swapped the C-terminal stalk region consisting of the thigh, calf-1, calf-2, transmembrane (TM), and cytoplasmic domains between αIIb and αV. The B/V chimera has αIIb β-propeller joined with αV stalk, whereas the V/B chimera has

[1] The abbreviations used are: Fbg, fibrinogen; EGF, epidermal growth factor; mAb, monoclonal antibody; FITC, fluorescein isothiocyanate; DTT, dithiothreitol; TM, transmembrane; βTD, β tail domain; CHO, Chinese hamster ovary.

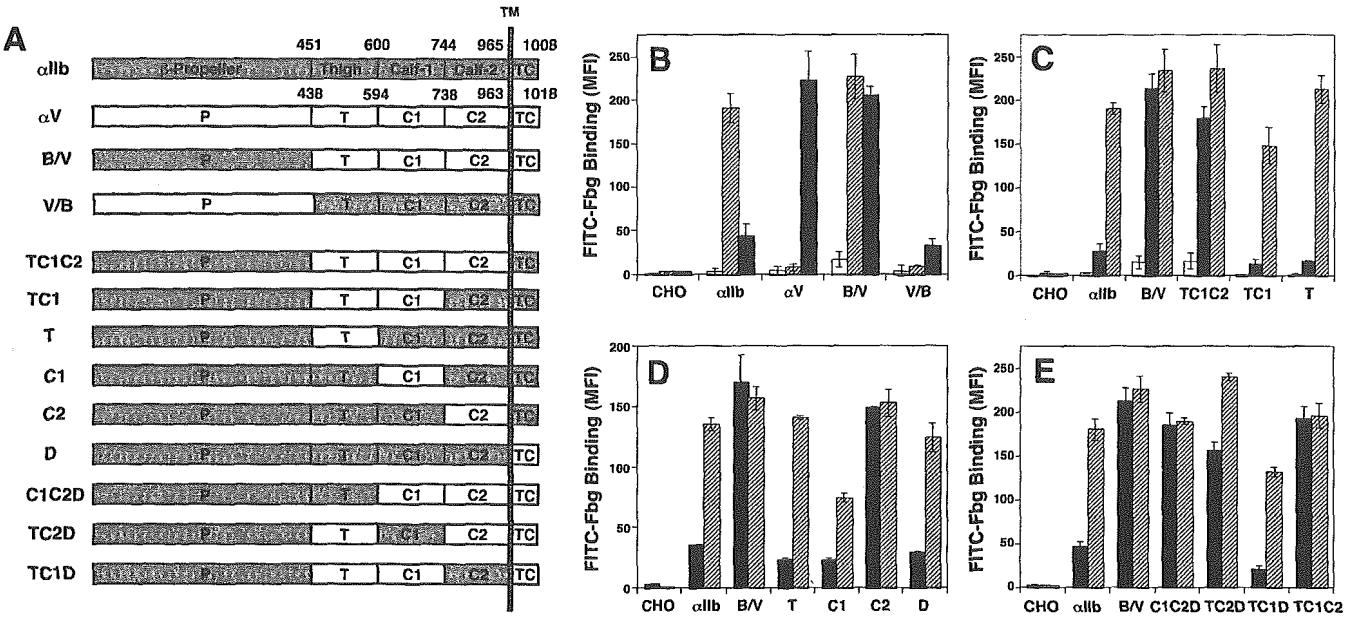

FIG. 1. **The calf-2 domain in integrin α subunit regulates Mn^{2+}-induced integrin activation.** *A*, schematic representation of the αIIb/αV chimeras. Positions of the domain boundaries are indicated. The specific binding of FITC-Fbg is presented in mean fluorescent intensity. *B*, FITC-Fbg binding to cells expressing α stalk-swapping chimeras (B/V and V/B) in the presence of 1 mM Ca^{2+}/Mg^{2+} (*open bar*), 1 mM Ca^{2+}/Mg^{2+} + 10 μg/ml PT25-2 (*cross-hatched bar*), and 1 mM Mn^{2+} (*filled bar*) is shown. *C*, FITC-Fbg binding to cells expressing αIIb/αV domain-swapping chimeras (TC1C2, TC1, and T) in the presence of 1 mM Ca^{2+}/Mg^{2+} (*open bar*) and 1 mM Mn^{2+} (*filled bar*) and cells pretreated with DTT in the presence of 1 mM Ca^{2+}/Mg^{2+} (*hatched bar*) is shown. *D* and *E*, FITC-Fbg binding to cells expressing αIIb/αV domain-swapping chimeras (T, C1, C2, D, C1C2D, TC2D, TC1D, and TC1C2) in the presence of 1 mM Mn^{2+} (*filled bar*) and cells pretreated with DTT in the presence of 1 mM Ca^{2+}/Mg^{2+} (*hatched bar*) is shown.

αV-propeller joined with αIIb stalk. In terms of cation-binding site, only the site at the junction between the thigh and the calf-1 domains is replaced in those chimeras, and the other four sites in the β-propeller domain remain unchanged (Fig. 1*A*). The chimeras were transiently expressed in CHO cells. Surface expression of each chimeric molecule was monitored using mAbs PL98DF6, P2, SZ21, PT25-2, OP-G2, and AMF-7. All chimeras showed mAb binding comparable with that of wild-type αIIbβ3 or αVβ3 (data not shown). In the presence of 1 mM Ca^{2+}/Mg^{2+} without any activators, none of the cells expressing chimeras including wild-type αIIbβ3 or αVβ3 significantly bound Fbg (Fig. 1*B*). In the presence of mAb PT25-2, which binds to αIIb β-propeller and activates αIIbβ3 (21–23), Fbg bound to wild-type αIIbβ3 and to B/V chimera, but not to wild-type αVβ3 or to V/B chimera. This is because this particular antibody is unable to bind to αVβ3 or V/B. In the presence of 1 mM Mn^{2+}, although αIIbβ3 did show some binding, it was not as avid as that seen in the presence of PT25-2. By contrast, Mn^{2+} induced robust Fbg binding to wild-type αVβ3. These results are in agreement with previous reports. However, when α stalk was swapped, the response to Mn^{2+} changed completely from the wild-type. The B/V bound Fbg just as avidly as wild-type αVβ3. By contrast, V/B binding significantly decreased to a level similar to that of wild-type αIIbβ3. These results clearly indicate that the integrin α stalk, but not the head, contains the critical component that regulates Mn^{2+}-induced integrin activation.

The αV Calf-2 Domain, Not the αIIb Calf-2 Domain, Facilitates Mn^{2+}-induced Activation—To locate the regulatory domain essential for Mn^{2+}-induced activation, we created nine additional domain-swapping chimeras (Fig. 1*A*). These chimeras were created based on the domain boundaries in the αVβ3 crystal structure (3). All of them have αIIb β-propeller on the N terminus. Thus, the ligand-binding domains remain unchanged. Each chimera was designated after the domain replaced, except for the D chimera, which has αV TM and cytoplasmic domains. The chimeras were transiently expressed in CHO cells. Surface expression of each chimera was comparable (data not shown). The first set of experiments showed that TC1C2 bound Fbg just as avidly as B/V in the presence of Mn^{2+} (Fig. 1*C*). However, Mn^{2+} did not induce Fbg binding in TC1 or T. When the cells were pretreated with DTT, which is known to activate integrin, all chimeras including TC1 and T showed Fbg binding comparable to that of wild-type αIIbβ3 in the presence of 1 mM Ca^{2+}/Mg^{2+}. These results suggest that the αV calf-2 domain, but not the αV TM or cytoplasmic domains, is required for Mn^{2+}-induced activation. It is worth noting that none of the chimeras induced constitutive activation. To determine whether αV calf-2 domain alone could facilitate αIIbβ3-Fbg interaction by Mn^{2+}, we swapped individual domains in the next set of experiments. Although swapping individual thigh (T), calf-1 (C1), and TM-cytoplasmic (D) domains had no effect, swapping calf-2 domain (C2) resulted in robust Fbg binding in the presence of Mn^{2+} (Fig. 1*D*). These results suggest that the αV calf-2 domain has a facilitating effect on ligand binding by Mn^{2+}, whereas the αIIb calf-2 domain lacks the same effect. To examine whether αIIb calf-2 domain alone could neutralize the activating effect of α stalk swapping, individual αIIb domain sequences were put back in the B/V chimera that shows Mn^{2+}-induced activation. When original αIIb thigh (C1C2D), calf-1 (TC2D), TM-cytoplasmic (TC1C2) domain sequences were put back in, they did not have a significant effect on Mn^{2+}-induced activation induced by α stalk swapping. However, when αIIb calf-2 domain sequences were put back in (TC1D), the Mn^{2+}-induced activation was completely lost (Fig. 1*E*). This suppressing effect was reversed by DTT treatment. These results suggest that the differences in the response to Mn^{2+} between αIIbβ3 and αVβ3 can be solely attributed to the calf-2 domain.

Mutation in the Cation-binding Site at α Genu Does Not Affect Mn^{2+}-induced Ligand Binding—In the αVβ3 crystal structure, the only cation-binding site in the α stalk is located at the junction between the thigh and the calf-1 domains, but not in the calf-2 domain. To examine the effect of this cation-binding site on ligand binding, Asp^{599} and Glu^{636}, which coor-

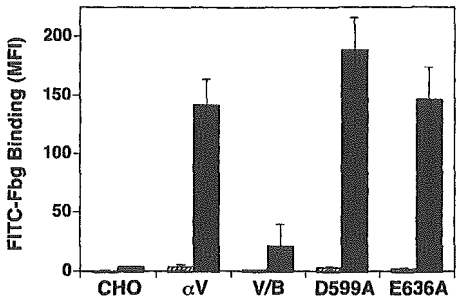

FIG. 2. **The effect of mutation in the cation-coordinating amino acid residues on the αVβ3-ligand interaction.** Asp^{599} and Glu^{636}, which coordinate a cation at αV genu, were individually mutated to Ala. FITC-Fbg binding to CHO cells expressing mutant αVβ3 in the presence of 1 mM Ca^{2+}/Mg^{2+} (*hatched bar*) and 1 mM Mn^{2+} (*filled bar*) is shown.

dinate a cation at αV genu, were mutated to Ala. These two acidic residues are conserved in most integrins. Mutating individual amino acid residues to Ala did not inhibit αVβ3-Fbg interaction induced by Mn^{2+} (Fig. 2). It did not induce constitutive activation in the presence of 1 mM Ca^{2+}/Mg^{2+}, either. Although these results do not rule out the possibility that this cation-binding site may play some role in ligand binding, they are consistent with the results obtained using domain-swapping chimeras.

Specific Amino Acid Residues at the Calf-2/EGF4-βTD Interface Regulate Mn^{2+}-induced Ligand Binding—In the αVβ3 crystal structure, the calf-2 domain creates a 700 Å interface with EGF4 and βTD (24). This implicates that the difference in the interaction between those membrane-proximal domains might affect Mn^{2+}-dependent integrin activation. To explore this possibility, we mutated amino acid residues in the αIIb calf-2 domain that make up the interface. Eight non-conserved amino acid regions (amino acids 747–749, 754–758, 770, 777–779, 783, 893–894, 896–898, and 954–956) that are located at the calf-2/EGF4-βTD interface in the αVβ3 crystal structure were selected. Amino acid sequences in the homologous αIIb regions (amino acids 753–755, 760–764, 774, 781–783, 787, 899–900, 902–904, and 958–960) were replaced with the corresponding αV sequences (designated B/V 753–755, B/V 760–764, B/V 774, B/V 781–783, B/V 787, B/V 899–900, B/V 902–904, and B/V 958–960, respectively). When expressed in CHO cells, all those mutants showed comparable surface expression with wild-type αIIbβ3, except for B/V 902–904, which showed significantly lower expression (data not shown). The DTT treatment induced comparable Fbg binding in all mutants except B/V 902–904. These results suggest that whereas B/V 902–904 has an unfavorable effect on the global structure of αIIbβ3, other mutations did not. In the presence of 1 mM Mn^{2+}, B/V 753–755, B/V 774, B/V 781–783, B/V 902–904, or B/V 958–960 showed comparable Fbg binding with wild-type αIIbβ3 (Fig. 3*A*). In contrast, B/V 787 and B/V 899–900 showed significantly higher Fbg binding. In addition, B/V 760–764 also showed weak but consistently higher Fbg binding than wild-type αIIbβ3. To further identify the amino acid residues in the 760–764 and 899–900 regions important for Mn^{2+}-induced Fbg binding, individual residues in these regions were mutated. None of the single amino acid mutations in the 760–764 region induced Fbg binding equivalent to B/V 760–764. On the contrary, mutating Arg^{900} to Ser alone was sufficient to induce Fbg binding equivalent to B/V 899–900 (Fig. 3*B*). However, none of those mutations produced Fbg binding as robust as C2. Next we examined whether combining those mutations would have an additive or synergistic effect. Combining B/V 787 mutation with the B/V 899–900 or B/V 900 mutation (designated B/V 787/899–900 and B/V 787/900, respectively) did not have any significant effect (Fig. 3*C*). The effect of combining B/V 760–764 mutation with B/V 787/899–900 (designated B/V 760–764/787/899–900) was additive and resulted in higher Fbg binding than any one of these mutants. These results indicate that whereas B/V 787 and B/V 900 have similar effects, B/V 760–764 has an independent effect on Mn^{2+}-induced Fbg binding. In the αVβ3 crystal structure, amino acid residues 783 and 894, which correspond to 787 and 900 in αIIb, are located next to each other and make contacts with the EGF4 domain, whereas 754–758, which corresponds to 760–764 in αIIb, is located close to the cell membrane and makes contacts with the βTD (Fig. 3*D*). These results indicate that the effect of calf-2 domain swapping on the Mn^{2+}-induced ligand interaction is mediated at least in part by the specific amino acid residues in the calf-2/EGF4-βTD interface, suggesting that differences in the calf-2/EGF4 and calf-2/βTD interface interaction in two β3 integrins are indeed responsible for the distinct response to Mn^{2+}. However, the fact that combining B/V 760–764, B/V 787, and B/V 899–900 mutations did not produce as much Fbg binding as C2 indicates that other amino acid residues in the calf-2 domain are involved. The positions of amino acid residues 839–867 in the αV calf-2 domain (842–873 in αIIb) have not been assigned in the αVβ3 crystal structure. This region may provide additional sites important for regulating integrin-ligand interaction.

Constraining the Calf-2/EGF4-βTD Interface in αVβ3 Inhibits its Mn^{2+}-induced Activation—If calf-2/EGF4-βTD interface interaction is involved in the regulation of Mn^{2+}-induced ligand binding, constraint in the interface should have a profound impact on integrin activation and conformation. To examine this hypothesis, we introduced an artificial disulfide bridge to put constraint in this interface. As seen in Fig. 4*A*, αV Ser^{749} and β3 Asp^{606} are physically close, and if these residues are mutated to Cys at the same time, we will be able to introduce a disulfide bridge. Although individual αV S749C or β3 D606C did not have any significant effect, double cysteine mutation 749/606 reduced Fbg binding to about one-third (Fig. 4*B*). This suppression was neutralized when the cells were treated with DTT to disrupt the disulfide bridge. These results suggest that restraining the possible movements in this membrane-proximal domain interface has a significant inhibitory effect on Mn^{2+}-induced integrin activation.

Next we examined the effect of the constraint on the conformational change of αVβ3. To monitor the conformational change, we examined the binding of anti-LIBS antibodies. The anti-LIBS mAbs bind preferentially to ligand-occupied form of integrins. Thus, they are believed to detect conformational changes associated with ligand binding (19). In this assay, the binding of non-functional anti-β3 mAb VNR5-2 did not change among those mutants. The presence of 1 mM GRGDS peptide did not significantly affect the binding, either (Fig. 4*C*). The binding of anti-LIBS1 was significantly weaker than that of VNR5-2. However, the binding of anti-LIBS1 showed a robust increase in the presence of 1 mM GRGDS peptide. No significant difference was observed among wild-type and cysteine mutants (Fig. 4*D*). By contrast, anti-LIBS2 binding in the presence of GRGDS peptide was suppressed in the double mutant (Fig. 4*E*). Although the localization of the epitope for anti-LIBS1 is not known, the epitope for anti-LIBS2 has been located within amino acid residues 602–690 in the βTD (25). These results suggest that the constraint on the membrane-proximal α/β interface restricts the conformational change within the membrane-proximal domain upon ligand binding. However, it may not prevent the conformational change in other parts of the molecule.

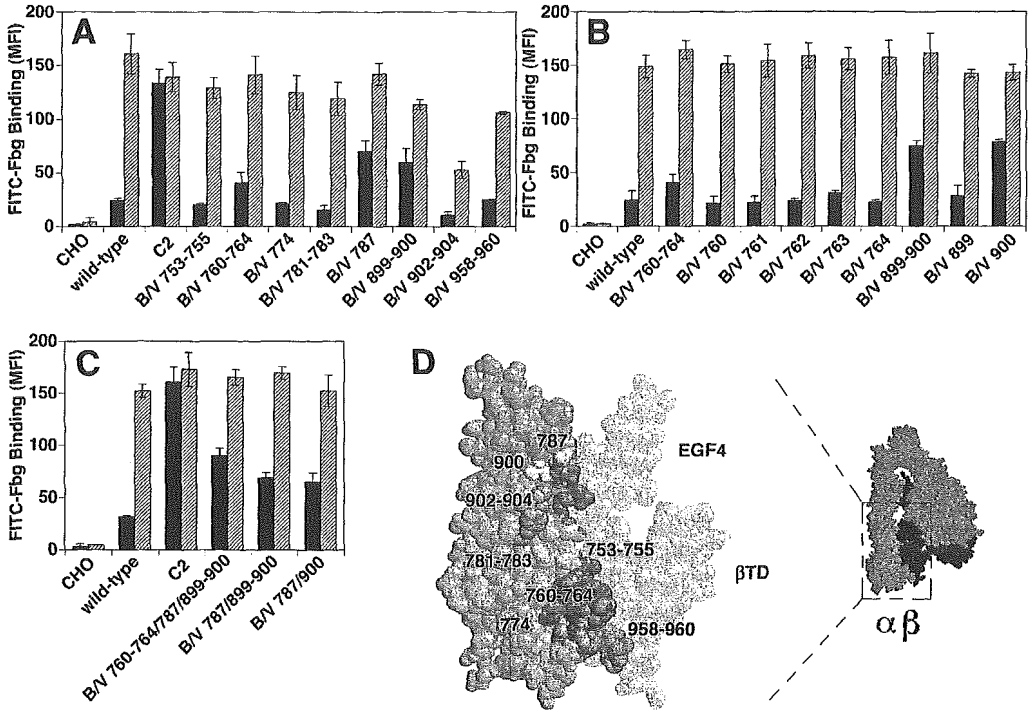

FIG. 3. **The effect of αIIb to αV mutation in amino acid residues located at the calf-2/EGF4-βTD interface on the αIIbβ3-ligand interaction.** *A*, amino acid residues 753–755, 760–764, 774, 781–783, 787, 899–900, 902–904, and 958–960 located at the calf-2/EGF4-βTD interface in αIIb were mutated to the corresponding residues in αV. The resulting αIIbβ3 mutants are designated B/V 753–755, B/V 760–764, B/V 774, B/V 781–783, B/V 787, B/V 899–900, B/V 902–904, and B/V 958–960, respectively. *B*, amino acid residues in the αIIb 760–764 and 899–900 regions were individually mutated to the corresponding residues in αV. *C*, B/V 760–764, B/V 787, and B/V 899–900 or B/V 900 mutations were combined. These αIIbβ3 mutants were expressed in CHO cells. FITC-Fbg binding to cells expressing αIIbβ3 in the presence of 1 mM Mn^{2+} (*filled bar*) and cells pretreated with DTT in the presence of 1 mM Ca^{2+}/Mg^{2+} (*hatched bar*) is shown. As a reference, Fbg binding to cells expressing wild-type αIIbβ3 and C2 chimera are also shown. *D*, the spacefill model of αVβ3 crystal structure. The αV chain is shown in *green*, and the β3 chain is shown in *red*. The membrane-proximal domains are magnified on the *left*. The calf-2 domain is shown in *light green*, and the EGF4 and βTD are shown in *transparent red*. Positions of amino acid residues corresponding to 753–755, 760–764, 774, 781–783, 787, 900, 902–904, and 958–960 in αIIb are shown and labeled. Amino acid residues 787/900 and 760–764, which promoted Mn^{2+}-induced Fbg binding when mutated to αV residue, are shown in *yellow* and *orange*, respectively. Amino acid residues 753–755, 774, and 781–783, which did not affect Fbg binding, are in *cyan*. Amino acid residues 902–904, which jeopardized surface expression and Fbg binding, are shown in *blue*. The models were created using RasMol.

Constraint in the Calf-2/EGF4-βTD Interface in αIIbβ3 Completely Abrogates Inside-out Signaling—We next examined the effect of this interdomain interaction on integrin activation induced by other stimuli. We introduced homologous cysteine mutation into αIIbβ3 and examined the effect on Fbg binding in the presence of 1 mM Ca^{2+}/Mg^{2+} (Fig. 5*A*). Without activators, none of those mutants bound Fbg. When activating mAb PT25-2 was included to enforce the conformational change of the extracellular domain in favor of ligand binding, wild-type (αIIb/β3) and individual cysteine mutants αIIb F755C (755/β3) and β3 D606C (αIIb/606) showed comparable Fbg binding. However, the Fbg binding to double cysteine mutant 755/606 showed a 50% decrease. The effect of the constraint was neutralized when the disulfide bridge was disrupted by prior treatment with DTT. These results suggest that constraining the membrane-proximal domain interface prevents integrin from achieving full activation, regardless of activators.

The effect of the constraint is far more dramatic in inside-out signaling. To mimic inside-out signaling, the cytoplasmic domain of β3 was truncated at the membrane-proximal Leu^{717} (26). The truncated αIIbβ3 (αIIb/β3tr) bound Fbg in the presence of Ca^{2+}/Mg^{2+} without any activators, as reported previously (Fig. 5*B*). When individual cysteine mutation αIIb F755C or β3 D606C was introduced in truncated αIIbβ3 (designated 755/β3tr and αIIb/606tr, respectively), it did not significantly block Fbg binding. In contrast, Fbg binding was completely abrogated in double cysteine mutant 755/606tr. Activating antibody did not override the inhibition completely. Fbg binding was completely restored only when the disulfide bridge was disrupted with DTT treatment. The cysteine mutations had similar effects when αIIbβ3 was activated by αIIb cytoplasmic domain truncation (Fig. 5*C*). Although individual αIIb F755C or β3 D606C mutation (775tr/β3 and αIIbtr/606, respectively) did not have a significant impact as compared with wild-type (αIIbtr/β3), double cysteine mutation 755tr/606 completely abrogated Fbg binding. This suppression was completely neutralized with DTT treatment. Thus, disruption of the membrane-proximal domain interface is essential for propagating inside-out signaling. These results suggest that constraining the membrane-proximal α/β interface not only restricts integrin activation by divalent cations but also prevents activation by inside-out signaling.

DISCUSSION

In this study, we provide evidence that interdomain interactions in the integrin stalk regions, particularly in the membrane-proximal domains, are the key regulator of integrin activation. By using Mn^{2+}-induced Fbg binding to β3 integrins as a model system, we demonstrated the following: 1) that switching α stalk region resulted in switching the Mn^{2+} requirement for ligand binding in αIIbβ3 and αVβ3, 2) that the calf-2 domain in the α stalk region is the sole determinant for the distinct response to Mn^{2+}, 3) that this response is mediated in part by the specific amino acid residues in the calf-2 domain that create the calf-2/EGF4-βTD interface, and 4) that constraining the calf-2/EGF4-βTD interface not only inhibited Mn^{2+}-induced integrin activation but also completely abrogated inside-out signaling. These results suggest that the ex-

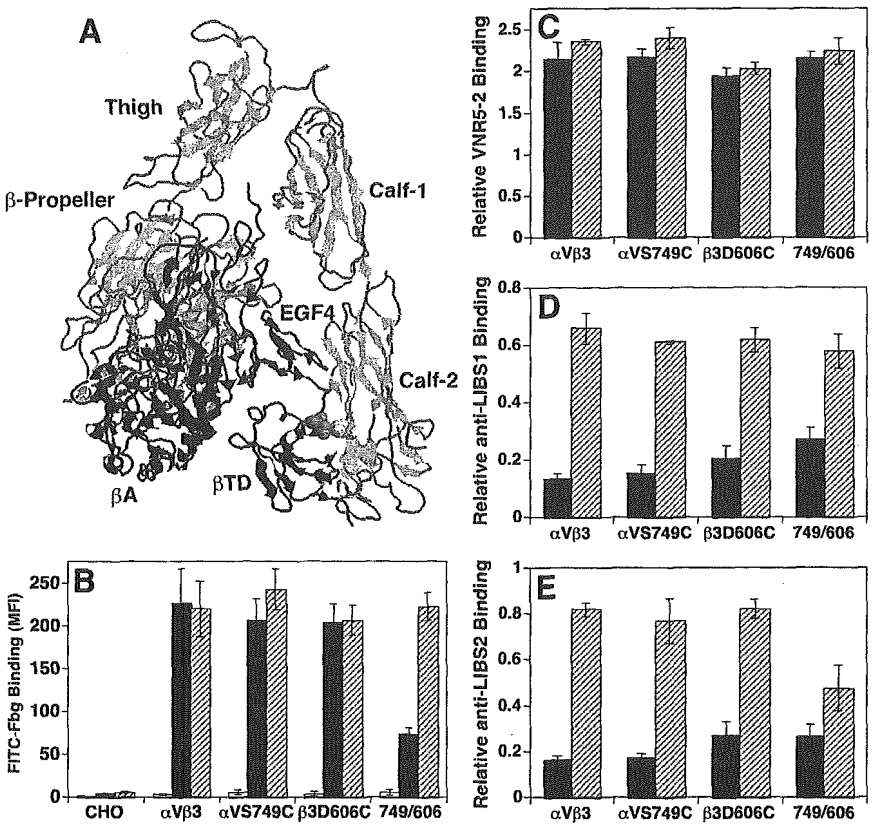

FIG. 4. **The effect of constraint in the membrane-proximal α/β interface in αVβ3 on ligand binding and conformation.** *A*, ribbon models depicting the crystal structure of the αVβ3 extracellular domain. The α and β subunits are shown in *cyan* and *red*, respectively. The amino acid residues Ser^{749} in αV and Asp^{606} in β3 that were mutated to Cys to facilitate disulfide bridge formation in the study are shown in *yellow* and *orange spacefills*, respectively. The model was created using RasMol. *B*, FITC-Fbg binding to cells expressing individual Cys mutant αVS749C, β3D606C, and double Cys mutant 749/606 in the presence of 1 mM Ca^{2+}/Mg^{2+} (*open bar*) and 1 mM Mn^{2+} (*filled bar*) and cells pretreated with DTT in the presence of 1 mM Mn^{2+} (*hatched bar*) is shown. *C–E*, mAb binding to cells expressing individual Cys mutant αVS749C, β3D606C, and double Cys mutant 749/606 in the presence 1 mM Ca^{2+}/Mg^{2+} (*filled bar*) and 1 mM Ca^{2+}/Mg^{2+} + 1 mM GRGDS peptide (*hatched bar*) is shown. Relative mAb binding was calculated as described under "Experimental Procedures." The binding of VNR5-2, anti-LIBS1, anti-LIBS2 is shown in *C*, *D*, and *E*, respectively.

tracellular, membrane-proximal α/β interaction plays important roles in regulating the cation-dependent integrin activation and critically controls the propagation of inside-out signaling.

Integrin α subunit contains five cation-binding sites. The four EF-hand-like motifs in α subunit previously predicted to bind Ca^{2+} form β hairpin loops and actually coordinate cations regardless of bound ligand (3). Although previous studies have shown that the Fbg γ-chain peptide cross-links to the second EF-hand-like motif in blade 5 of the αIIb-propeller (27), mutational studies suggest these sites are not likely to contain a major ligand-binding site (28, 29). In addition, conservative Asp/Asn to Glu mutations in the four EF-hand-like motifs in α4β1 had no effect on the binding of soluble ligand (30). Consistently, these β hairpin loops are all located opposite to the β-propeller/βA interface that comprises the ligand binding face. Our results using α stalk-swapping mutants suggest that the β-propeller domain does not contain a regulatory site for Mn^{2+}-induced Fbg binding, but the α stalk does. Indeed, the α stalk contains the fifth cation-binding site at the junction between the thigh and calf-1 domains. This site is located at the α genu, where integrin makes a 135° bend in the crystal structure. It has been predicted that a cation bound to this site may help neutralize the negative charge in the thigh/calf-1 interface in an extended conformer (3). Thus, it is tempting to speculate that this cation-binding site may regulate Mn^{2+}-induced ligand binding by controlling the transition from bent to extended conformer. However, our results suggest this is not the case. Instead, results from the domain-swapping chimeras indicate that the C-terminal α calf-2 domain plays a critical role in regulating integrin activation.

Several lines of evidence implicate the role of the calf-2 domain in integrin activation. Some integrin α subunit is proteolytically cleaved into covalently linked heavy and light chains during post-translational processing. Prevention of this endoproteolytic cleavage by mutagenesis abrogated α6β1 activation by phorbol myristate acetate (31). Neutrophil elastase cleaves αIIb between Val^{837} and Asp^{838}, close to the endoproteolytic cleavage site in the calf-2 domain (32). Although the elastase does not, by itself, induce platelet aggregation, it greatly potentiates αIIbβ3 activation by cathepsin G and Mn^{2+} (17, 33). Thus, structural alterations in the calf-2 domain affect integrin activation. Conversely, ligand binding provokes structural change in the calf-2 domain. Upon ligand binding, the integrin stalk regions express neo-epitopes that are recognized by a group of anti-LIBS mAbs. These epitopes are mostly located in the β stalk region (25, 34). Notably, one such mAb, PMI-1, recognizes an epitope within residues 842–856 of the αIIb calf-2 domain (35). Thus, structural change in the calf-2 domain is closely associated with integrin activation. How does the calf-2 domain affect Mn^{2+}-induced Fbg binding, despite the fact that it does not contain actual cation-binding sites? Previous studies suggest that the membrane-proximal α/β interaction modulates integrin affinity regulation by divalent cations. Kinetic studies using recombinant truncated α5β1 and αVβ3 with an artificial C-terminal clasp suggest that α/β interaction in the TM and cytoplasmic domains decreases integrin affinity by increasing the dissociation rate. Electron microscopic observation revealed that the two stalks are widely separated at their ends in unclasped α5β1 (36), whereas they are still connected at their ends in a majority of molecules in unclasped recombinant αVβ3, even in the presence of Mn^{2+} (4). These reports suggest that the extracellular, membrane-proximal α/β interface formation is significant in some integrins under physiological conditions and may account for the distinct response to Mn^{2+} in β3 integrins. Indeed, αIIb to αV mutation in selected amino acid residues that make up the calf-2/EGF4 and calf-2/βTD interface greatly facilitated Mn^{2+}-induced Fbg binding in αIIbβ3. Stabilizing this interface with a disulfide bridge (749/606 mutant) prevented Mn^{2+}-induced Fbg binding to αVβ3. It is possible that constraining the membrane-proximal α/β interface may somehow constrain integrin in a bent

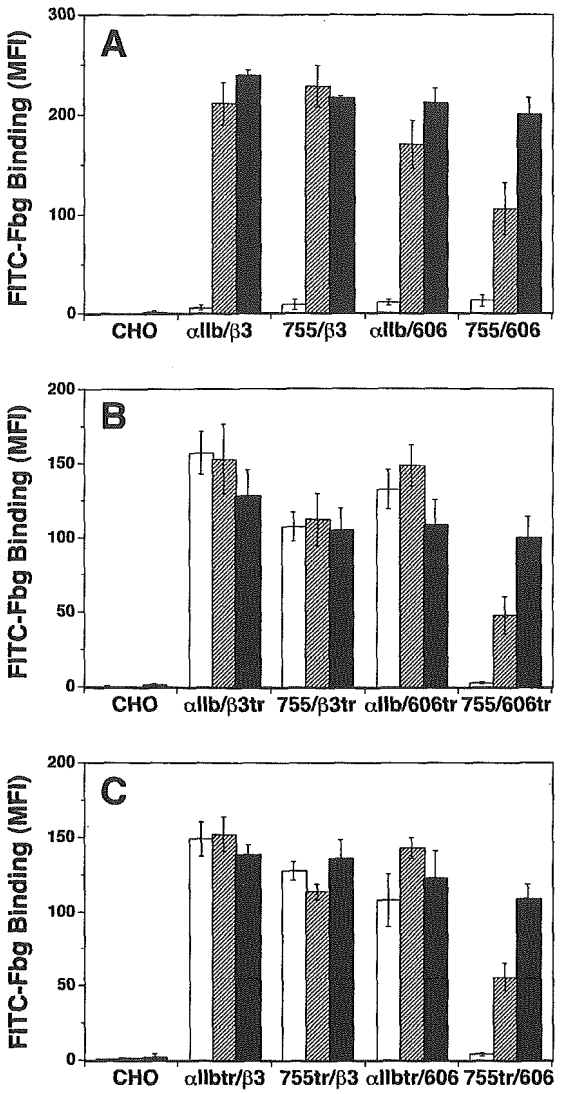

FIG. 5. **The effect of constraint in the membrane-proximal α/β interface on ligand binding to αIIbβ3.** *A*, amino acid residue Phe[755] in αIIb, which is homologous to Ser[749] in αV, was mutated to Cys (F755C) to facilitate disulfide bridge formation between αIIb and β3. FITC-Fbg binding to cells expressing αIIbβ3 (*αIIb/β3*) carrying individual αIIb F755C mutation (*755/β3*), β3 D606C mutation (*αIIb/606*), and double αIIb F755C and β3 D606C mutation (*755/606*) in the presence of 1 mM Ca^{2+}/Mg^{2+} (*open bar*) and 1 mM Ca^{2+}/Mg^{2+} plus 10 μg/ml PT25-2 (*hatched bar*) and cells pretreated with DTT in the presence of 1 mM Ca^{2+}/Mg^{2+} (*filled bar*) is shown. *B*, to mimic inside-out signaling, β3 was truncated at Leu[717] by introducing a stop codon in β3 cDNA (β3tr). The D606C mutation was introduced in β3tr (606tr). Wild-type αIIb or αIIb carrying F755C mutation was expressed together with β3tr or 606tr in CHO cells. FITC-Fbg binding to cells expressing truncated αIIbβ3 (*αIIb/β3tr*) carrying αIIb F755C mutation (*755/β3tr*), β3 D606C mutation (*αIIb/606tr*), and αIIb F755C and β3 D606C mutations (*755/606tr*) in the presence of 1 mM Ca^{2+}/Mg^{2+} (*open bar*) and 1 mM Ca^{2+}/Mg^{2+} plus 10 μg/ml PT25-2 (*hatched bar*) and cells pretreated with DTT in the presence of 1 mM Ca^{2+}/Mg^{2+} (*filled bar*) is shown. *C*, to mimic inside-out signaling, αIIb was truncated at Gly[991] by introducing a stop codon in αIIb cDNA (αIIbtr). The F755C mutation was introduced in αIIbtr (755tr). Wild-type β3 or β3 carrying the D606C mutation was expressed together with αIIbtr or 755tr in CHO cells. FITC-Fbg binding to cells expressing truncated αIIbβ3 (*αIIbtr/β3*) carrying αIIb F755C mutation (*755tr/β3*), β3 D606C mutation (*αIIbtr/606*), and αIIb F755C and β3 D606C mutations (*755tr/606*) in the presence of 1 mM Ca^{2+}/Mg^{2+} (*open bar*) and 1 mM Ca^{2+}/Mg^{2+} plus 10 μg/ml PT25-2 (*hatched bar*) and cells pretreated with DTT in the presence of 1 mM Ca^{2+}/Mg^{2+} (*filled bar*) is shown.

state, thereby keeping integrin in a low affinity state. However, the 749/606 and 755/606 double mutants did undergo conformational change upon ligand binding, as detected by LIBS epitope expression. These mutants still showed some Fbg binding when stimulated by Mn^{2+} or activating mAb. In contrast, constraining the integrin in a bent state by introducing a disulfide bridge between βA and βTD resulted in failure to induce LIBS epitope expression upon ligand binding and complete loss of ligand binding, even in the presence of activating mAb.[2] Thus, constraining the α/β stalks and β head/β stalk has a distinct conformational effect on integrin structure. In addition, the fact that extended, clasped conformer can be observed under electron microscopy (4) indicates that constraining the α/β stalks does not necessarily constrain integrin in a bent state. On the contrary, disruption of the membrane-proximal α/β interface may lead to integrin activation. Anti-LIBS2 that binds to βTD has been shown to activate αIIbβ3 (25). Likewise, two mAbs that bind to αIIb calf-2 domain weakly induced Fbg binding in the presence of Ca^{2+}/Mg^{2+}. Notably, these mAbs potentiated Mn^{2+}-induced Fbg binding.[3] Disruption of the Cys^{608}-Cys^{655} and Cys^{663}-Cys^{687} disulfide bridges in βTD that face the calf-2/EGF4-βTD interface in the crystal structure constitutively activated αIIbβ3, whereas disruption of the other two disulfide bridges did not (37). These results implicate that the membrane-proximal calf-2/EGF4-βTD interface may act as a physiological clasp and thus regulate integrin activation.

Integrin stalks also make interface at calf-1/EGF3, TM domains, and cytoplasmic tails. Previous studies suggest that α/β interaction in TM domain and cytoplasmic tail, as well as the interaction of cytoplasmic tails with actin cytoskeleton, is important for restraining integrins in low affinity form (38–41). These membrane-proximal interactions probably act in concert to maintain integrin in the default low affinity state because disruption of any of these interactions makes the integrin prone to activation. This may explain why the detergent-solubilized or truncated recombinant αIIbβ3 is able to bind ligands without activation, whereas intact heterodimers on the platelet surface are not able to do so. Among α/β interfaces, calf-2/EGF4-βTD is unique because only the calf-2 domain (and not the thigh, calf-1, or TM-cytoplasmic domains) displayed a significant difference in promoting Mn^{2+}-induced integrin activation, suggesting that this interface is much more stable in αIIbβ3 than in αVβ3. The divergent nature of the calf-2/EGF4-βTD interface interaction among integrins may be responsible for the different LIBS epitope expression in β1 integrins in response to ligand or Mn^{2+} occupancy (42). Thus, the calf-2/EGF4-βTD interaction may differentially regulate ligand interaction and conformational change in integrins.

In inside-out signaling, how the interactions within the short cytoplasmic tails trigger structural rearrangements in the large extracellular domain remains a mystery. The cytoplasmic, membrane-proximal interaction constrains integrin in an inactive state (40). Recently, the talin head domain has been shown to activate αIIbβ3 by disrupting the membrane-proximal αIIb/β3 tail interface *in vitro* (43). In living cells, the αL/β2 cytoplasmic tails undergo separation upon agonist stimulation (44). Conversely, in outside-in signaling, ligand binding induces a structural rearrangement in the cytoplasmic tails and induces separation of the tails (44) and exposure of the LIBS epitope in α tail (45). Our results unequivocally indicate that separation of the cytoplasmic tails is unable to induce integrin activation unless the extracellular stalks separate from each other. In agreement, previous studies have shown that αIIbβ3 stalks undergo structural rearrangement and

[2] T. Kamata, M. Handa, Y. Ikeda, and S. Aiso, manuscript in preparation.

[3] T. Kamata, M. Handa, Y. Ikeda, and S. Aiso, unpublished observations.